

THE THERMAL EFFECTS ON SURFACE FAILURE IN GEARS



BY ERNEST ATAN

A DISSERTATION PRESENTED TO THE GRADUATE SCHOOL
OF THE UNIVERSITY OF FLORIDA IN PARTIAL FULFILLMENT
OF THE REQUIREMENTS FOR THE DEGREE OF
DOCTOR OF PHILOSOPHY

UNIVERSITY OF FLORIDA

2003

I dedicate this thesis to my dear father, mother, wife and son....

ACKNOWLEDGMENTS

I would like to thank my advisor, Dr. Ali A. Saeed, for the excellent education that I have received under his direction. His scientific legacy is unmatched. His support for my study is greatly appreciated.

I would also like to acknowledge the members of my committee: Dr. Joseph Duffy who unfortunately passed away before the defense of my dissertation; Carl G. Crone; John E. Salvatore; Edward K. Walsh; and John C. Zenger for their professional advice and suggestions about my research. My special thanks extend to Dr. Adam Degan for his help.

I also would like to thank my family for their great support during every stage of my studies.

TABLE OF CONTENTS

	Page
ACKNOWLEDGMENTS	iii
LIST OF TABLES	vi
LIST OF FIGURES	viii
ABSTRACT	xiii
CHAPTERS	
1 INTRODUCTION	1
Fring and Ryeon Studies on Friling of Rolling/Sliding Contacts	1
Wear and Ryeon Studies on Wear of Rolling/Sliding Contacts	1
Scoring and Ryeon Studies on Scoring of Rolling/Sliding Contacts	4
Studies on Surface Temperature Characteristics of Sliding/Rolling Contacts	5
Overview of the Study	6
2 DIMENSIONLESS RELATIONSHIP FOR SURFACE TEMPERATURE	7
Nominal Temperature Rise at The Start of Contact Zone	7
Dimensionless Temperature, Rise and The Thermal Stress	12
Dimensionless Contact Stress (Mechanical Stress)	13
3 DIMENSIONLESS RELATIONSHIP FOR CONTACT STRESS DISTRIBUTION	15
Thermal Stress	15
Thermal Fringe	16
Thermal Shock	17
Indurance Limit	18
Combined Thermal and Mechanical Stress Effects on Fringe	19
Modification of Mechanical Stress/Combined with Thermal Stress	40

4 INVESTIGATION OF THE EFFECT OF SURFACE ROUGHNESS AND LUBRICATION ON MAXIMUM TEMPERATURE IN THE CONTACT ZONE	75
Lubricating Film	79
Maximizing Pressure and Surface Roughness	77
The Contact Between Rough Surfaces	88
Coefficients of Friction of Lubricated Sliding/Rolling Contact	92
Temperature Rise Calculations in Lubricated Rough Surface Contact	94
Applications to Gears	96
Material Remelt	97
Contact Stress Modification Factor in Lubricated Rolling/Sliding Contact	99
5 SUMMARY, CONCLUSION AND RECOMMENDATIONS	109
Summary	118
Conclusions	120
Recommendation	121
LIST OF REFERENCES	140
BIOGRAPHICAL SKETCH	146

LIST OF TABLES

Table	Page
2-1 Temperature rise values versus load and number of teeth for $(C_d)=18$ in. $M_g=12$	28
2-2 Temperature rise values versus load and number of teeth for $(C_d)=18$ in. $M_g=15$	28
2-3 Temperature rise values versus load and number of teeth for $(C_d)=18$ in. $M_g=18$	29
2-4 Temperature rise values versus load and number of teeth for $(C_d)=20$ in. $M_g=21$	29
2-5 Temperature rise values versus load and number of teeth for $(C_d)=20$ in. $M_g=24$	30
2-6 Temperature rise values versus load and number of teeth for $(C_d)=20$ in. $M_g=30$	30
2-7 Temperature rise values versus load and number of teeth for $(C_d)=20$ in. $M_g=33$	31
2-8 Temperature rise values versus load and number of teeth for $(C_d)=20$ in. $M_g=35$	31
2-9 Temperature rise values versus load and number of teeth for $(C_d)=20$ in. $M_g=38$	31
2-10 Dimensionless temperature rise values versus gear ratios and number of teeth for $(C_d)=20$ in. load $(W_d)=1000$ lb.	31
2-11 Material thermal stress values for temperature rise values versus gear ratios and number of teeth for $(C_d)=20$ in. load $(W_d)=1000$ lb.	31
2-12 Dimensionless mechanical stress values versus gear ratios and number of teeth for $(C_d)=20$ in. load $(W_d)=1000$ lb.	31
3-1 Factors K_1 , K_2 for combined mechanical and thermal fatigue for 4140 high carbon steel and 1020 low carbon steel	61
3-2 Design factor $1/\sqrt{1+K}$ versus load and number of teeth for $(C_d)=18$ in. $M_g=12$	66
3-3 Design factor $1/\sqrt{1+K}$ versus load and number of teeth for $(C_d)=20$ in. $M_g=21$	66
3-4 Design factor $1/\sqrt{1+K}$ versus load and number of teeth for $(C_d)=20$ in. $M_g=24$	67

3-3 Design factor $(\frac{1}{\sqrt{1+K}})$ versus load and number of teeth for $(C_p=10 \text{ in.}, M_g=5) \dots 67$

3-4 Design factor $(\frac{1}{\sqrt{1+K}})$ versus load and number of teeth for $(C_p=10 \text{ in.}, M_g=6) \dots 68$

3-5 Design factor $(\frac{1}{\sqrt{1+K}})$ versus load and number of teeth for $(C_p=10 \text{ in.}, M_g=7) \dots 68$

3-6 Design factor $(\frac{1}{\sqrt{1+K}})$ versus load and number of teeth for $(C_p=10 \text{ in.}, M_g=8) \dots 69$

3-7 Design factor $(\frac{1}{\sqrt{1+K}})$ versus load and number of teeth for $(C_p=10 \text{ in.}, M_g=9) \dots 69$

3-8 Design factor $(\frac{1}{\sqrt{1+K}})$ versus load and number of teeth for $(C_p=10 \text{ in.}, M_g=10) \dots 70$

3-9 Design factor $(\frac{(\sigma_a - \sigma_c)}{\sqrt{1+K}})$ versus load and number of teeth for $(C_p=10 \text{ in.}, M_g=1) \dots 70$

3-10 Design factor $(\frac{(\sigma_a - \sigma_c)}{\sqrt{1+K}})$ versus load and number of teeth for $(C_p=10 \text{ in.}, M_g=2) \dots 71$

3-11 Design factor $(\frac{(\sigma_a - \sigma_c)}{\sqrt{1+K}})$ versus load and number of teeth for $(C_p=10 \text{ in.}, M_g=3) \dots 71$

3-12 Design factor $(\frac{(\sigma_a - \sigma_c)}{\sqrt{1+K}})$ versus load and number of teeth for $(C_p=10 \text{ in.}, M_g=4) \dots 72$

3-13 Design factor $(\frac{(\sigma_a - \sigma_c)}{\sqrt{1+K}})$ versus load and number of teeth for $(C_p=10 \text{ in.}, M_g=5) \dots 72$

3-14 Design factor $(\frac{(\sigma_a - \sigma_c)}{\sqrt{1+K}})$ versus load and number of teeth for $(C_p=10 \text{ in.}, M_g=6) \dots 73$

3-15 Design factor $(\frac{(\sigma_a - \sigma_c)}{\sqrt{1+K}})$ versus load and number of teeth for $(C_p=10 \text{ in.}, M_g=7) \dots 73$

3-16 Design factor $(\frac{(\sigma_a - \sigma_c)}{\sqrt{1+K}})$ versus load and number of teeth for $(C_p=10 \text{ in.}, M_g=8) \dots 74$

3-17 Design factor $(\frac{(\sigma_a - \sigma_c)}{\sqrt{1+K}})$ versus load and number of teeth for $(C_p=10 \text{ in.}, M_g=9) \dots 74$

4-1 Roughness and profile data for typical farming operations	111
4-2 Generalized/Williamson model input parameters calculated for surface roughness data present (Table 4-1).....	111
4-3 Lubricating oil and material thermal and mechanical properties	112
4-4 Temperature rise on surface, asperities and lubricant film temperatures versus number of teeth for fine ground, load 50 hp., Gear ratio $M_g=2$, center distance C _D =18 and constant oil viscosity at inlet temperature	113
4-5 Temperature rise on surface, asperities and lubricant film temperatures versus number of teeth for fine ground, load 50 hp., Gear ratio $M_g=5$, center distance C _D =18 and constant oil viscosity at inlet temperature	113
4-6 Temperature rise on surface, asperities and lubricant film temperatures versus number of teeth for fine ground, load 50 hp., Gear ratio $M_g=10$, center distance C _D =18 and constant oil viscosity at inlet temperature	114
4-7 Temperature rise on surface, asperities and lubricant film temperatures versus number of teeth for rough ground, load 50 hp., Gear ratio $M_g=2$, center distance C _D =18 and constant oil viscosity at inlet temperature	114
4-8 Temperature rise on surface, asperities and lubricant film temperatures versus number of teeth for rough ground, load 50 hp., Gear ratio $M_g=5$, center distance C _D =18 and constant oil viscosity at inlet temperature	115
4-9 Temperature rise on surface, asperities and lubricant film temperatures versus number of teeth for rough ground, load 50 hp., Gear ratio $M_g=10$, center distance C _D =18 and constant oil viscosity at inlet temperature	115
4-10 Temperature rise on surface, asperities and lubricant film temperatures versus number of teeth for fine ground, load 50 hp., gear ratio $M_g=2$, center distance C _D =18 and constant oil viscosity at maximum surface temperature	116
4-11 Temperature rise on surface, asperities and lubricant film temperatures versus number of teeth for fine ground, load 50hp., gear ratio $M_g=5$, center distance C _D =18 and constant oil viscosity at maximum surface temperature	116
4-12 Temperature rise on surface, asperities and lubricant film temperatures versus number of teeth for fine ground, load 100hp., gear ratio $M_g=5$, center distance C _D =18 and constant oil viscosity at maximum surface temperature	117
4-13 Temperature rise on surface, asperities and lubricant film temperatures versus number of teeth for rough ground, load 50 hp., gear ratio $M_g=2$, center distance C _D =18 and constant oil viscosity at maximum surface temperature	117

4-14 Temperature rises on surfaces, asperities and lubricant film temperatures versus number of teeth for rough ground, lead 30/40, gear ratio Mg=3, center distance Cd=10 and constant oil viscosity at maximum surface temperature	118
4-15 Temperature rises on surfaces, asperities and lubricant film temperatures versus number of teeth for rough ground, lead 30/40, gear ratio Mg=10, center distance Cd=10 and constant oil viscosity at maximum surface temperature	119
4-16 Temperature rises on asperities versus number of teeth and lead for fine ground, gear ratio Mg=2, center distance Cd=10 and constant oil viscosity at inlet temperature	119
4-17 Temperature rises on asperities versus number of teeth and lead for fine ground, gear ratio Mg=10, center distance Cd=10 and constant oil viscosity at inlet temperature	119
4-18 Temperature rises on asperities versus number of teeth and lead for rough ground, gear ratio Mg=2, center distance Cd=10 and constant oil viscosity at inlet temperature	120
4-19 Temperature rises on asperities versus number of teeth and lead for rough ground, gear ratio Mg=10, center distance Cd=10 and constant oil viscosity at inlet temperature	120
4-20 Temperature rises on asperities versus number of teeth and lead for fine ground, gear ratio Mg=2, center distance Cd=10 and constant oil viscosity at maximum surface temperature	121
4-21 Temperature rises on asperities versus number of teeth and lead for fine ground, gear ratio Mg=10, center distance Cd=10 and constant oil viscosity at maximum surface temperature	121
4-22 Temperature rises on asperities versus number of teeth and lead for rough ground, gear ratio Mg=2, center distance Cd=10 and constant oil viscosity at maximum surface temperature	122
4-23 Temperature rises on asperities versus number of teeth and lead for rough ground, gear ratio Mg=10, center distance Cd=10 and constant oil viscosity at maximum surface temperature	122
4-24 Factor K, versus number of teeth and lead for rough ground and 4340 high-carbon steel gear, gear ratio Mg=2, center distance Cd=10 and constant oil viscosity at inlet temperature	123
4-25 Factor K, versus number of teeth and lead for rough ground and 4340 high-carbon steel gear, gear ratio Mg=10, center distance Cd=10 and constant oil viscosity at inlet temperature	123

4-26 Factor K, versus number of teeth and load for fine ground and 4340 high carbon steel gear, gear ratio Mg=2, center distance Cd=18 and constant oil viscosity at inlet temperature	128
4-27 Factor K, versus number of teeth and load for fine ground and 4340 high carbon steel gear, gear ratio Mg=18, center distance Cd=18 and constant oil viscosity at inlet temperature	128
4-28 Factor K, versus number of teeth and load for rough ground and 1020 low carbon steel gear, gear ratio Mg=2, center distance Cd=18 and constant oil viscosity at inlet temperature	128
4-29 Factor K, versus number of teeth and load for rough ground and 1020 low carbon steel gear, gear ratio Mg=18, center distance Cd=18 and constant oil viscosity at inlet temperature	128
4-30 Factor K, versus number of teeth and load for fine ground and 1020 low carbon steel gear, gear ratio Mg=2, center distance Cd=18 and constant oil viscosity at inlet temperature	128
4-31 Factor K, versus number of teeth and load for fine ground and 1020 low carbon steel gear, gear ratio Mg=18, center distance Cd=18 and constant oil viscosity at inlet temperature	128
4-32 Factor K, versus number of teeth and load for rough ground and 4340 high carbon steel gear, gear ratio Mg=2, center distance Cd=18 and constant oil viscosity at maximum surface temperature	127
4-33 Factor K, versus number of teeth and load for rough ground and 4340 high carbon steel gear, gear ratio Mg=18, center distance Cd=18 and constant oil viscosity at maximum surface temperature	127
4-34 Factor K, versus number of teeth and load for fine ground and 4340 high carbon steel gear, gear ratio Mg=2, center distance Cd=18 and constant oil viscosity at maximum surface temperature	128
4-35 Factor K, versus number of teeth and load for fine ground and 4340 high carbon steel gear, gear ratio Mg=18, center distance Cd=18 and constant oil viscosity at maximum surface temperature	128
4-36 Factor K, versus number of teeth and load for rough ground and 1020 low carbon steel gear, gear ratio Mg=2, center distance Cd=18 and constant oil viscosity at maximum surface temperature	128
4-37 Factor K, versus number of teeth and load for rough ground and 1020 low carbon steel gear, gear ratio Mg=18, center distance Cd=18 and constant oil viscosity at maximum surface temperature	128

4-38 Factor K , versus number of teeth and load for fine ground and 1450 low carbon steel gear, gear ratio $M_g=1$, center distance $C_d=18$ and constant oil viscosity at maximum surface temperature	130
4-39 Factor K , versus number of teeth and load for fine ground and 1450 low carbon steel gear, gear ratio $M_g=10$, center distance $C_d=18$ and constant oil viscosity at maximum surface temperature	130
4-40 Design factor $1/\sqrt{Y+K}$, versus number of teeth and load for rough ground and 4340 high carbon steel gear, gear ratio $M_g=1$, center distance $C_d=10$ and constant oil viscosity at inlet temperature	131
4-41 Design factor $1/\sqrt{Y+K}$, versus number of teeth and load for rough ground and 4340 high carbon steel gear, gear ratio $M_g=10$, center distance $C_d=10$ and constant oil viscosity at inlet temperature	131
4-42 Design factor $1/\sqrt{Y+K}$, versus number of teeth and load for fine ground and 4340 high carbon steel gear, gear ratio $M_g=1$, center distance $C_d=18$ and constant oil viscosity at inlet temperature	132
4-43 Design factor $1/\sqrt{Y+K}$, versus number of teeth and load for fine ground and 4340 high carbon steel gear, gear ratio $M_g=10$, center distance $C_d=10$ and constant oil viscosity at inlet temperature	132
4-44 Design factor $1/\sqrt{Y+K}$, versus number of teeth and load for rough ground and 1020 low carbon steel gear, gear ratio $M_g=1$, center distance $C_d=18$ and constant oil viscosity at inlet temperature	133
4-45 Design factor $1/\sqrt{Y+K}$, versus number of teeth and load for rough ground and 1020 low carbon steel gear, gear ratio $M_g=10$, center distance $C_d=18$ and constant oil viscosity at inlet temperature	133
4-46 Design factor $1/\sqrt{Y+K}$, versus number of teeth and load for fine ground and 1020 low carbon steel gear, gear ratio $M_g=1$, center distance $C_d=18$ and constant oil viscosity at inlet temperature	134
4-47 Design factor $1/\sqrt{Y+K}$, versus number of teeth and load for fine ground and 1020 low carbon steel gear, gear ratio $M_g=10$, center distance $C_d=18$ and constant oil viscosity at inlet temperature	134
4-48 Design factor $1/\sqrt{Y+K}$, versus number of teeth and load for rough ground and 4340 high carbon steel gear, gear ratio $M_g=1$, center distance $C_d=18$ and constant oil viscosity at maximum surface temperature	135

4-58 Design factor $\frac{1}{\sqrt{Q(1+K)}}$ versus number of teeth and load for rough ground and 4340-high carbon steel gear, gear ratio Mg=10, center distance Cd=10 and constant oil viscosity at maximum surface temperature	115
4-59 Design factor $\frac{1}{\sqrt{Q(1+K)}}$ versus number of teeth and load for fine ground and 4340-high carbon steel gear, gear ratio Mg=2, center distance Cd=10 and constant oil viscosity at maximum surface temperature	116
4-60 Design factor $\frac{1}{\sqrt{Q(1+K)}}$ versus number of teeth and load for fine ground and 4340-high carbon steel gear, gear ratio Mg=10, center distance Cd=10 and constant oil viscosity at maximum surface temperature	116
4-61 Design factor $\frac{1}{\sqrt{Q(1+K)}}$ versus number of teeth and load for rough ground and 1020 low carbon steel gear, gear ratio Mg=2, center distance Cd=10 and constant oil viscosity at maximum surface temperature	117
4-62 Design factor $\frac{1}{\sqrt{Q(1+K)}}$ versus number of teeth and load for rough ground and 1020 low carbon steel gear, gear ratio Mg=10, center distance Cd=10 and constant oil viscosity at maximum surface temperature	117
4-63 Design factor $\frac{1}{\sqrt{Q(1+K)}}$ versus number of teeth and load for fine ground and 1020 low carbon steel gear, gear ratio Mg=2, center distance Cd=10 and constant oil viscosity at maximum surface temperature	118
4-64 Design factor $\frac{1}{\sqrt{Q(1+K)}}$ versus number of teeth and load for fine ground and 1020 low carbon steel gear, gear ratio Mg=10, center distance Cd=10 and constant oil viscosity at maximum surface temperature	118

LIST OF FIGURES

Figure	Page
2-1 Working bend of test versus non-interactive model	13
2-2 Ratio of invariant of working tooth profiles	14
2-3 Temperature map plot versus load and number of teeth for $(C_{27}=10 \text{ in.}, \text{Mg}=2)$	17
2-4 Temperature map plot versus load and number of teeth for $(C_{27}=10 \text{ in.}, \text{Mg}=5)$	18
2-5 Temperature map plot versus load and number of teeth for $(C_{27}=10 \text{ in.}, \text{Mg}=10)$	19
2-6 Temperature map plot versus load and number of teeth for $(C_{27}=20 \text{ in.}, \text{Mg}=2)$	20
2-7 Temperature map plot versus load and number of teeth for $(C_{27}=20 \text{ in.}, \text{Mg}=5)$	21
2-8 Temperature map plot versus load and number of teeth for $(C_{27}=20 \text{ in.}, \text{Mg}=10)$	22
2-9 Temperature map plot versus load and number of teeth for $(C_{27}=30 \text{ in.}, \text{Mg}=2)$	23
2-10 Temperature map plot versus load and number of teeth for $(C_{27}=30 \text{ in.}, \text{Mg}=5)$	24
2-11 Temperature map plot versus load and number of teeth for $(C_{27}=30 \text{ in.}, \text{Mg}=10)$	25
2-12: a) Maximal thermal stress and b) Mechanical contact stress plots versus gear ratios and number of teeth for $(C_{27}=10 \text{ in.}, \text{Load} (\text{N}) = 1000 \text{ lb.})$	26
2-13: a) Dimensionless thermal and b) Dimensionless mechanical stress plots versus gear ratios and number of teeth for $(C_{27}=30 \text{ in.}, \text{Load} (\text{N}) = 1000 \text{ lb.})$	27
3-1 Typical endurance stress curve (S-N)	43
3-2 Fatigue data for 4140 steel (High carbon) [37]	44
3-3 Fatigue data for 1020 low carbon steel [37]	45
3-4 Design approach plot	56
3-5 Ultimate strength change versus temperature (in)	66

3-6 Design factor $\sqrt{\frac{\sigma_m - \sigma_c}{(1 + K_s)}}$ versus load and number of teeth for $(C_D=1 \text{ in.}, Mg=2) \dots 43$

3-7 Design factor $\sqrt{\frac{\sigma_m - \sigma_c}{(1 + K_s)}}$ versus load and number of teeth for $(C_D=2 \text{ in.}, Mg=2) \dots 44$

3-8 Design factor $\sqrt{\frac{\sigma_m - \sigma_c}{(1 + K_s)}}$ versus load and number of teeth for $(C_D=3 \text{ in.}, Mg=2) \dots 45$

3-9 Design factor $\sqrt{\frac{\sigma_m - \sigma_c}{(1 + K_s)}}$ versus load and number of teeth for $(C_D=4 \text{ in.}, Mg=2) \dots 46$

3-10 Design factor $\sqrt{\frac{\sigma_m - \sigma_c}{(1 + K_s)}}$ versus load and number of teeth for $(C_D=5 \text{ in.}, Mg=2) \dots 47$

3-11 Design factor $\sqrt{\frac{\sigma_m - \sigma_c}{(1 + K_s)}}$ versus load and number of teeth for $(C_D=6 \text{ in.}, Mg=2) \dots 48$

3-12 Design factor $\sqrt{\frac{\sigma_m - \sigma_c}{(1 + K_s)}}$ versus load and number of teeth for $(C_D=7 \text{ in.}, Mg=2) \dots 49$

3-13 Design factor $\sqrt{\frac{\sigma_m - \sigma_c}{(1 + K_s)}}$ versus load and number of teeth for $(C_D=8 \text{ in.}, Mg=2) \dots 50$

3-14 Design factor $\sqrt{\frac{\sigma_m - \sigma_c}{(1 + K_s)}}$ versus load and number of teeth for $(C_D=9 \text{ in.}, Mg=2) \dots 51$

3-15 Design factor $\frac{(\sigma_m - \sigma_c)}{\sqrt{(1 + K_s)}}$ versus load and number of teeth for $(C_D=1 \text{ in.}, Mg=3) \dots 56$

3-16 Design factor $\frac{(\sigma_m - \sigma_c)}{\sqrt{(1 + K_s)}}$ versus load and number of teeth for $(C_D=2 \text{ in.}, Mg=3) \dots 57$

3-17 Design factor $\frac{(\sigma_m - \sigma_c)}{\sqrt{(1 + K_s)}}$ versus load and number of teeth for $(C_D=3 \text{ in.}, Mg=3) \dots 58$

3-18 Design factor $\frac{(\sigma_m - \sigma_c)}{\sqrt{(1 + K_s)}}$ versus load and number of teeth for $(C_D=4 \text{ in.}, Mg=3) \dots 59$

3-19 Design factor $\frac{(\sigma_m - \sigma_c)}{\sqrt{(1 + K_s)}}$ versus load and number of teeth for $(C_D=5 \text{ in.}, Mg=3) \dots 60$

3-20 Design factor $\frac{(\sigma_m - \sigma_c)}{\sqrt{(1 + K_s)}}$ versus load and number of teeth for $(C_D=6 \text{ in.}, Mg=3) \dots 61$

3-21 Design factor $\frac{(\sigma_m - \sigma_c)}{\sqrt{(1 + K_s)}}$ versus load and number of teeth for $(C_D=7 \text{ in.}, Mg=3) \dots 62$

3-22 Design factor $\frac{\left(\frac{S_{ut}}{F_T}\right)\left(\frac{S_{ut}}{F_T}\right)}{\sqrt{(1+K)}}$ versus load and number of teeth for $(C_L=30 \text{ in.}, Mg=10)$	67
3-23 Design factor $\frac{\left(\frac{S_{ut}}{F_T}\right)\left(\frac{S_{ut}}{F_T}\right)}{\sqrt{(1+K)}}$ versus load and number of teeth for $(C_L=30 \text{ in.}, Mg=10)$	68
4-1 Rough surface in contact.....	90
4-2 Variation of coefficient of friction with sliding rate; $N_1=0.100 \text{ m/sec}$ (2T).....	91
4-3 Coefficient of friction at $d_o/R_2=0$ against normal d_o/R (2T).....	91
4-5 Proposed effective surface roughness for various manufacturing (2T).....	92
4-6 Effective $(d_o/R)_e$ against normal d_o/R (2T).....	92
4-7 Lubricated heavily loaded sliding/rolling contact (26).....	93
4-8 Flow chart of temperature rise calculation, where viscosity constant at maximum method.....	94
4-9 Design factor $\frac{1}{\sqrt{(1+K)}}$ versus number of teeth and load for rough ground and 4140 high carbon steel gear gear ratio $Mg=2$, center distance $CD=10$ and constant oil viscosity at inlet temperature.....	95
4-10 Design factor $\frac{1}{\sqrt{(1+K)}}$ versus number of teeth and load for rough ground and 4140 high carbon steel gear gear ratio $Mg=10$, center distance $CD=10$ and constant oil viscosity at inlet temperature.....	96
4-11 Design factor $\frac{1}{\sqrt{(1+K)}}$ versus number of teeth and load for fine ground and 4140 high carbon steel gear gear ratio $Mg=2$, center distance $CD=10$ and constant oil viscosity at inlet temperature.....	97
4-12 Design factor $\frac{1}{\sqrt{(1+K)}}$ versus number of teeth and load for fine ground and 4140 high carbon steel gear gear ratio $Mg=10$, center distance $CD=10$ and constant oil viscosity at inlet temperature.....	98
4-13 Design factor $\frac{1}{\sqrt{(1+K)}}$ versus number of teeth and load for rough ground and 1020 low carbon steel gear gear ratio $Mg=2$, center distance $CD=10$ and constant oil viscosity at inlet temperature.....	99
4-14 Design factor $\frac{1}{\sqrt{(1+K)}}$ versus number of teeth and load for rough ground and 1020 low carbon steel gear gear ratio $Mg=10$, center distance $CD=10$ and constant oil viscosity at inlet temperature.....	100

4-15 Design factor $\frac{1}{\sqrt{f(1+K)}}$ versus number of teeth and load for fine ground and 1020 low carbon steel gear, gear ratio $M_g=2$, center distance $CD=10$ and constant oil viscosity at ambient temperature	101
4-16 Design factor $\frac{1}{\sqrt{f(1+K)}}$ versus number of teeth and load for fine ground and 1020 low carbon steel gear, gear ratio $M_g=12$, center distance $CD=10$ and constant oil viscosity at ambient temperature	102
4-17 Design factor $\frac{1}{\sqrt{f(1+K)}}$ versus number of teeth and load for rough ground and 4140 high carbon steel gear, gear ratio $M_g=2$, center distance $CD=10$ and constant oil viscosity at maximum surface temperature	103
4-18 Design factor $\frac{1}{\sqrt{f(1+K)}}$ versus number of teeth and load for rough ground and 4140 high carbon steel gear, gear ratio $M_g=20$, center distance $CD=10$ and constant oil viscosity at maximum surface temperature	104
4-19 Design factor $\frac{1}{\sqrt{f(1+K)}}$ versus number of teeth and load for fine ground and 4140 high carbon steel gear, gear ratio $M_g=12$, center distance $CD=10$ and constant oil viscosity at maximum surface temperature	105
4-20 Design factor $\frac{1}{\sqrt{f(1+K)}}$ versus number of teeth and load for fine ground and 4140 high carbon steel gear, gear ratio $M_g=10$, center distance $CD=10$ and constant oil viscosity at maximum surface temperature	106
4-21 Design factor $\frac{1}{\sqrt{f(1+K)}}$ versus number of teeth and load for rough ground and 1020 low carbon steel gear, gear ratio $M_g=2$, center distance $CD=10$ and constant oil viscosity at maximum surface temperature	107
4-22 Design factor $\frac{1}{\sqrt{f(1+K)}}$ versus number of teeth and load for rough ground and 1020 low carbon steel gear, gear ratio $M_g=12$, center distance $CD=10$ and constant oil viscosity at maximum surface temperature	108
4-23 Design factor $\frac{1}{\sqrt{f(1+K)}}$ versus number of teeth and load for fine ground and 1020 low carbon steel gear, gear ratio $M_g=2$, center distance $CD=10$ and constant oil viscosity at maximum surface temperature	109
4-24 Design factor $\frac{1}{\sqrt{f(1+K)}}$ versus number of teeth and load for fine ground and 1020 low carbon steel gear, gear ratio $M_g=12$, center distance $CD=10$ and constant oil viscosity at maximum surface temperature	110

*A Report of Dissertation Presented to the Graduate School
of the University of Florida in Partial Fulfillment of the
Requirements for the Degree of Doctor of Philosophy*

THERMAL EFFECTS ON SURFACE FAILURE IN Gears

By

Drishkar Anu

August 2002

Chairman: Ali A. Seiring

Major Department: Mechanical Engineering

Advances standards and design relationships for surface durability of gears are based on various stress considerations. Thermal effects are considered only for scoring failures when the destruction of the lubricating film occurs as a result of temperature rise. Temperature increase on the surface reduces the film thickness and causes the solid to solid contact. The objectives of this dissertation are to consider the mechanism of thermal stress and thermal cycling during tooth contacts for dry and lubricated conditions and its effect on the allowable mechanical and thermal strength for different manufacturing processes and geometrical conditions. The main goal is to develop a dimensionless relationship to take into consideration the combined effect of the thermal and mechanical stress in predicting the surface failure of gears for different design, manufacturing and operating parameters. The result of the study shows that the gears with low number of pinion teeth and high pressure are most influenced by the thermal effects. Also the allowable mechanical stress is reduced with decreasing center distance. The surface roughness is found to have a significant effect on the temperature rise on specimens but

not on the bulk surface. Fine ground gears are generally less affected by the thermal stress since the heat input is far in excess there. High carbon steel gears are significantly more sensitive to the thermal stress than low carbon steel because of the significant change of their ultimate strength with temperature and their high susceptibility to thermal fatigue and thermal shock.

CHAPTER 1 INTRODUCTION

Although most of the failures of gears are surface failures, the connection between the factors influencing these failures is not yet fully understood. Furthermore, there is no general agreement among the researchers on the effect of lubrication on surface durability. The most common types of surface failures are usually classified as pitting wear and scoring.

Pitting and Scoring, Similar to Pitting of Rolling-Contact Contacts

In the past there was a tendency to regard pitting as a secondary wear problem and most of the attention focused on macroscopic pitting, which is attributed to contact fatigue. Pitting is traditionally considered as a Hertzian fatigue phenomenon which occurs when a fatigue crack is initiated either at the surface of the gear tooth or at a small depth below the surface. It is seen in rolling element bearing and gears when the Hertzian pressure exceeds an allowable value. The crack usually propagates for a short distance in a direction roughly parallel to the tooth surface before turning up or branching to the surface. When the cracks grow to the extent of separating a piece of the surface material, a pit is formed. When several pits grow together, a larger pit is generally referred to as a "spall." Metallographic sections and other methods of examination suggest that the micro-pitting cracks and the cracks producing macro-scale pitting have similar morphology. The main difference seems to be that all scale

Webster and Hurlbut [1] investigated the effect of various parameters on a type of progressive fatigue wear known as macro-pitting. They concluded that increasing the

load decreasing, specific film thickness and maintaining negative relative sliding all increased the rate of stress-rupture tests. They also reported that stress-rupture is almost completely eliminated at very low, but non-zero, slide in roll rates.

Tollins [2] investigated the role of surface defects in spalling, life prediction modeling. His efforts concentrated on stress spalling, in fatigue circumstances. He analyzed surface distress defect formation in rolling contact using the Greenwood-Williamson surface roughness model. He suggests a significant influence on life of several parameters such as CPB, film thickness ratio, traction, material fatigue properties and pre service defects. In another paper, Tollins [3] proposed a spalling fatigue life model based on populations of surface defects with depth (severity) distribution according to the Greenwood-Williamson severity model.

Chen [4] concluded from experimental tests that pitting failure is liable to occur on the contacting parts with a rougher surface. Chen, Cheng, and Chen [5] presented a finite stress tensor model for surface pitting in rolling and sliding contact. They analyzed the parameters related to severity interaction and the subsurface stress map along the whole contact area by superimposing the severity loads on the Hertzian load for a given specimen surface.

Blake and Chang [6-7] reported on a surface pitting life model for estimating failure probabilities and service lives of spur gears based on an initial crack size distribution and an parallel interaction between cracks and inclusion. An improved model was suggested by Blake and Dempster [8]. The two-dimensional propagation model was modified to reflect three dimensional cracks driven by both shear and lubricant pressure effects.

Wear and Oros [9] measured some tests to examine the influence of lubricants on copper-rolling. Ping, Jones, and Salovei [10] investigated the behavior of subsurface cracks in steel tests. They constructed a finite element model of a number of two-dimensional cracks beneath the pitch line of a gear tooth.

Wear and Recent Studies on Wear of Rolling/Sliding Contacts

Wear is a surface phenomenon in which layers of metal are removed or "worn away" from its free surfaces from the contacting surfaces of the gear teeth. Experience indicates that metal is removed in the pitting areas where the maximum negative sliding occurs at the starting point of contact. The pitch line appears to show no subsurface loss. Wear is most commonly assumed to be caused by repeated dislocations of the fractured bonds and an inadequate lubrication film. Because the events that produce wear debris occur at and below the interface of contacting asperities, what is known about wear has been characterized by examining the products of wear, such as wear scars, debris, scars, thermal effects, hardness change, etc.

Adhesive wear (sometimes called scuffing or galling) involves material usage. First, when two surfaces are pressed together, the microscopic bumps on the surfaces separate together and form a solid junction when the motion of the two surfaces ceases. When one surface moves relative to the other, the weaker material breaks at some distance from the junction and forms a lump of worn material.

Abrasive wear occurs when a hard particle digs into a softer surface and plows out material. This is called two-body abrasion. Three-body abrasion may happen when free particles are trapped between the two surfaces. As the surfaces move relative to each other, the hard foreign particles plow out material from the softer surface areas. Other

situations are known to occur where the hard bearing particles are embedded in the softer material and create wear tracks on the harder surface.

Lin, Cheng, and Jeng [11] conducted experiments to measure the wear behavior of diamond lubricated gear contacts. They reported that the effect of applied load on wear is more significant than the effect of speed. They also reported that the oil temperatures increased as the sliding speed or the applied loads are increased.

Kopf [12] investigated the phenomenon of progressive wear, which causes a rapid increase in wear rate, distortion of the tooth profile and the failure of the gear transmission.

Makichukov [13] proposed a gear tooth wear analysis method that accounts for the change of the slip coefficient and the width of the contact area as it passes the working location of the tooth wear is determined. He reported that wear at the pitch point of an involute gear tooth was increased with an increase in the gear ratio.

Brondino et al. [14] reported on a method for the calculation of the work capacity of gear transmissions and proposed a wear contact based study on mechanical considerations. Formulas are proposed in their report for calculation of wear intensity of teeth.

Scoring and Pitting Resulting in Scoring of Rolling/Sliding Contacts

Scoring was often caused from a failure of the oil film due to overheating of the main generating heat in metal contacts. The contact produces extreme rubbing and scoring which removes metal rapidly from the sliding surfaces accompanied by transfer of metal from one surface to the other surface. This occurs at high sliding velocities and intense surface pressures, which cause the frictional heat. Failure of the lubricant is associated with a high temperature of the lubricant. The flash temperature is an

simultaneous temperature rise that occurs on the gear tooth surface due to the frictional heating.

Lee and Cheng [15–18] proposed a theory for predicting the onset of scoring failures over a wide range of operating conditions, including constant operating on the boundary lubrication and on the partial elasto-hydrodynamic lubrication regions. They concluded that failure occurs when the contact temperatures exceed a certain critical value. Experiments were undertaken [17] to support their hypothesis. Terauchi [18] reported on extensive experiments on the failure of the tooth surfaces of gear gears due to scoring. He examined the main factors influencing the scoring resistance of the gears, such as the number of teeth, tooth profile modifications, modules, and the mechanical and thermal properties of the gear materials and the lubricants.

Matsumoto [19] suggested that unit power is a viable scoring criterion for the surfaces of different materials under boundary lubrication conditions. Unger and Ku [20] proposed a methodology based on the critical thermal power criterion for explaining and predicting the scuffing behavior of sliding-rolling disks. Bell, Ojima, and Badley [21] investigated the independent influences of rolling speed and sliding speed on the scuffing of hardened steel discs lubricated by a mineral oil.

Marphanton and Cameron [22] investigated the phenomenon of fatigue scoring. They suggest that it is caused by micro-cracks and stress pits forming on the surface of heavily loaded contacts, which then erode the top of the contact.

Steady-State Thermal Temperature Calculation of Sliding/Rolling Contacts

Terauchi and Aoki [23] performed line tooth temperature analysis using a finite element method combined with a caloric coefficient approach, and examined how module coefficients. They also conducted experimental measurements of the average surface

temperatures and instantaneous surface temperatures. Chao, Fujita, and Pap [14, 25] investigated the temperature rise (the flash-temperature component) and the bulk temperature rise component) of a gear tooth model when a moving heat source with variable heat quantity radiates periodically at regular time intervals. Ashted and Boring [26] studied the heat partition and the transient temperature distribution in beveled concentrated contacts and developed the empirical formulas based on the numerical results for study.

Overview of the Study

All current standards and design relationships for surface durability of gears are based on fatigue stress considerations. Thermal effects are considered only for scoring failures when the destruction of the lubricating film occurs as a result of temperature rise.

The proposed study considers the mechanisms of thermal stress and thermal cycling during tooth contacts for dry and lubricated conditions and its effect on the ultimate mechanical and thermal strength for different machining processes and geometrical conditions. The main goal is to develop dimensionless relationships to take into consideration the combined effect of the thermal and mechanical stress on predicting the surface failure of gears for different design, manufacturing and operating parameters.

CHAPTER 2 DIMENSIONLESS RELATIONSHIP FOR SURFACE TEMPERATURE

Nominal 2 important Result: The State of Contact Zone

In order to investigate the surface damage phenomenon of gear teeth in contact, it would first be necessary to calculate the induced thermal and mechanical stresses at the most critical points of the contact cycle. The contact between the pinion and gear teeth surface can be considered as the contact of two cylinders with the same radii of curvature as the tooth surfaces at the contact zone.

The nominal temperature, T_n , is given as the sum of the bulk temperature (T_b) and the temperature rise (ΔT) due to frictional heating,

$$T_n = T_b + \Delta T \quad (2.1)$$

The induced temperature by a moving heat of heat source on semi infinite solid which can be applied to gears in sliding contact, is given by the solution of the governing differential equation for the one-dimensional heat conduction equation (22)

$$p \frac{\partial T}{\partial t} = k \frac{\partial}{\partial y} \left(k \frac{\partial T}{\partial y} \right) \quad (2.2a)$$

where t = time, sec

T = temperature, $^{\circ}\text{F}$

y = coordinate perpendicular to the plane of heat source, in.

p = material density lb/in^3

k = coefficient of conductivity $\text{in-lb/(sec)}^{\circ}\text{F}$

The boundary conditions for half-space are

$$t \text{ at } 0, \quad T(0, 0) = T_0 \text{ (Bulk temperature)}$$

On the surface of the solid the equation relating the constant electrical power intensity q to the temperature is written as

$$q \left(\frac{\partial T(0, 0)}{\partial y} \right) = \frac{1}{\alpha}$$

When the effect of the applied heat flux reaches the penetration depth (ΔT) the boundary condition expressing the heat transfer for zero heat flux across the lower plane boundary is expressed as

$$\left(\frac{\partial T(\Delta T, 0)}{\partial y} \right) = 0$$

The solution of the governing differential equation gives the maximum transient temperature at the contact zone as

$$\Delta T^* = \frac{2q}{\sqrt{\pi k \rho c}} \sqrt{t} \quad (2.14)$$

where, q = frictional heat flux

r = the mean diameter for heat flux application

k = thermal conductivity of the surface material

ρ = density

c = heat capacity

The frictional temperature rise for the pinion and gear at the point of contact, where the maximum sliding velocity and temperature rise occurs, can be determined by assuming two cylinders with radii corresponding to the radii of-curvature of the teeth as

the contact point. For two cylinders in contact, as shown in figure 2.2, the distance of contact for pinion teeth and gear teeth are

$$b_p = b/V_p \quad \text{and} \quad b_g = b/V_g \quad (2.10)$$

where b is the contact breadth as given by

$$b = \sqrt{\frac{16}{\pi} W_p R_p \left(\frac{1 - \nu_p^2}{E_p} + \frac{1 - \nu_g^2}{E_g} \right)} \quad (2.11)$$

and the surface velocities of pinion and gear can be calculated as

$$\begin{aligned} V_p &= \omega_p R_p (1 + M_p) \sin \phi \\ V_g &= \omega_g R_g \frac{(1 + M_g)}{M_g} (1 - x) \sin \phi \end{aligned} \quad (2.12)$$

where M_p = the equivalent radius of curvature

x = the relative position along the line of action, measured from the pinion base circle

M_g = gear ratio

It is generally known that most gear surface failures are seen at the start of contact

where the maximum temperature rise occurs due to the maximum heat generation

Therefore in this study only the start of the contact point is considered.

The relative position of contact at the start of contact can be written as

$$x_p = 1 - \frac{\sqrt{\left[M_p + \frac{1}{M_p} \right]^2 - M_p^2 \cos^2 \phi}}{(1 + M_g) \sin \phi} \quad (2.13)$$

It can be assumed that the contact bandwidth and the velocities do not change during the traversal of the contact band at a particular position of contact because of the small changes in the relative position coordinates.

The total heat flux, which depends on the work in overcoming friction and area generated inside the contact zone from the sliding contact of two teeth by friction, is defined as the energy generated per unit time due to friction,

$$q_t = \mu W_n V_s \quad (2.1)$$

The heat flux generated per unit length will be

$$q = f \frac{W_n}{b} V_s \quad (2.2)$$

where q = the frictional power intensity

f = coefficient of friction

W_n = the normal force per unit width on the surface

V_s = sliding velocity

b = width of contact band

The equation (2.2) can be applied for the start of contact as the position and gear by combining equations (2.1) & (2) as follows in four groups of parameters:

Material parameters $\rho_1, \rho_2, E, \mu, \nu$

Geometry parameters $\phi_b, \phi_d, N, \phi, \nu_d$

Lubrication and surface parameters $\mu_0, \mu, f, A_0, A_1, A_2, \nu$

Application parameters $\phi_1, \mu P, \omega_1, C_{12}$

$$dE^{-1} \rho_1 \nu_1 \rho_2 \nu_2 E, \mu, \phi_b \phi_d \phi_1 \phi_2 \nu, \phi, \nu_d, \mu_0 \mu, f, A_0, A_1, A_2 \phi_1 \phi_2 (\mu P, \omega_1, C_{12}) \quad (2.3)$$

$$\sigma_{\text{eq}} = \frac{1}{\sqrt{2}} \left[\left(1 + \frac{q_1}{K_1} + \frac{1 - q_1}{K_2} \right)^2 + \left(\frac{(1 + q_1)^2 q_1 (K_2 - K_1) \omega^2 v_p}{K_1 K_2 (1 - q_1) \omega^2 v_g} \right)^2 + \left(\frac{(1 - q_1)^2 q_1 (K_2 - K_1) \omega^2 v_p}{K_1 K_2 (1 - q_1) \omega^2 v_g} \right)^2 \right]^{1/2} \quad (2.96)$$

$$\sigma_{\text{eq}} = \frac{1}{\sqrt{2}} \left[\left(1 + \frac{q_1}{K_1} + \frac{1 - q_1}{K_2} \right)^2 + \left(\frac{(1 + q_1)^2 q_1 (K_2 - K_1) \omega^2 v_p}{K_1 K_2 (1 - q_1) \omega^2 v_g} \right)^2 + \left(\frac{(1 - q_1)^2 q_1 (K_2 - K_1) \omega^2 v_p}{K_1 K_2 (1 - q_1) \omega^2 v_g} \right)^2 \right]^{1/2} \quad (2.96)$$

where q_1 = first position of q to the pinion tooth surface

f = coefficient of friction between pinion-gear surfaces

A_o/A_p = ratio of real area of contact to nominal area of contact

The lubrication and the surface roughness parameters $q_1, f, A_o/A_p$ are evaluated for each case as shown in 4. In this chapter they are assumed to be constant. For the practical range of oil film thickness and some pinion and gear material the first position for the pinion and gear is $q=0.5$ [27].

The temperature rise values for gear stress $M_g=2.1$ and 18, contact distance $C_p=18, 25$ and 35 inches, and different power between 10 to 100 Hp are calculated and given in tables 2.1-2.9 and plotted in figures 2.3-2.18.

It can be seen from the figures that the temperature rises are significantly increased for low numbers of teeth and high gear stress. The decrease of contact distance also increases the temperature rises. Therefore the temperature rise should be given serious consideration for low numbers of teeth and the high gear stress.

Dimensionless Temperature Rise and The Thermal Stress

Dimensionless equations will be used to compare the relative importance of the thermal effects to the mechanical effects. Dimensionless temperature rise equation is defined as below by using average bulk temperature:

$$\Delta T_b / \Delta T_s = \frac{dP_{fr} \sqrt{dC_p}}{\rho(f \rho_s W^2 R_s)^{1/2}} \quad (2.10)$$

where, ΔT_b = instantaneous bulk temperature as defined in equation (2.9),

ρ = gear material mass density

k = gear material thermal conductivity,

c = gear material's specific heat density,

f = coefficient of friction,

R_s = modulus of elasticity,

W = tangential speed,

P_{fr} = integrated load per unit length of contact

C_p = center distance.

Dimensionless temperature rise values are calculated for center distances, C_p = 20 in. gear ratios, $M_g = 1, 2, 4, 10$ and number of teeth ranging between 17 and 34 with W = 1200 in. and ω_g = 1400 rpm. The results are given in table 2-10 and plotted in figure 2-12. Thermal stress will be evaluated based on the maximum thermal gradient, which occurs during the mesh.

The thermal stress for fatigue obtained as the maximum instantaneous temperature rise can be calculated by using the equations given in Refs. [28]

$$\sigma_{th} = \frac{E_p \rho_p \Delta T}{(1 + \nu_p)^2} \quad (2.11)$$

where α_p = thermal expansion coefficient

ν_p = poisson's ratio of piston material

Equation (7.11) is used to calculate the overall thermal stress in the assembly caused by the transient temperature rise induced by frictional or viscous heat input. In this chapter, only the frictional heat input with a constant coefficient of friction is considered. The change of the coefficient of friction and the viscous heat input when there is no metal-to-metal contact is analyzed in Chapter 4.

The considered examples are for gear ratio 1:2, 4 and 10 and center distance 30 mm with 50-100 teeth. The results are given in table 2-11 and plotted in figure 2-13. It can be seen from the calculated results that the thermal stress increases with increasing gear ratio and decreases with increasing number of teeth.

Discontinuous Contact Stress (Mechanical Stress)

The maximum Hertzian contact stress ($\sigma_{H\max}$) on gear tooth surface and the contact width (b) are given below with the assumption that Poisson's ratio is 0.3 [17]

$$\sigma_{H\max} = 0.394 \sqrt{\frac{E_1 E_2}{L_1 + L_2}} \quad (2.12)$$

$$b = 1.13 \sqrt{\frac{E_1 E_2}{L_1 + L_2}} \quad (2.13)$$

where $L_1 = \frac{E_1 F_1}{E_1 + \nu_1}$ and $L_2 = \frac{E_2 F_2}{E_2 + \nu_2}$

The discontinuous normal contact stress for the piston can therefore be derived, and function of number of piston tooth and gear ratio is

$$f_1(p, \nu_p) = \frac{\sigma_{H\max}}{E_1} \left(\frac{E_1}{E_2} \right)^{0.5} \quad (2.14)$$

The results for mechanical contact stress and dimensionless mechanical stress are given in tables 2-12 and 2-13 and plotted in figures 2-12 and 2-13 for the same input values given in the previous example for calculations of thermal stress.

The dimensionless ratio (normalized thermal stress / normalized mechanical stress) can be expressed as:

$$f_2(f_{2m}, M_p) = \frac{f_2(f_{2m}, M_p)}{f_2(f_{2m}, M_p)} \quad (2-15)$$

The dimensionless stress ratio can be calculated from the values of the dimensionless thermal stress- $Q_2(N_p, M_p)$ given in table 2-10 and the mechanical stress- $Q_2(N_p, M_p)$ given in table 2-13. The results, which are given in table 2-14, show that the thermal stress can play an important role in surface failure and should not be ignored in performance evaluation of the gears.

The following data are used for the performed calculations:

Gear parameters:

$$M_p = 1.2618$$

$$C_d = 10 \text{ m}$$

$$\text{Pinion rotational speed } \omega_p = 1000 \text{ rpm}$$

$$\text{Tooth load } (F_t) = 1000 \text{ N/m}$$

Material parameters:

$$E_{steel} = 206 \times 10^9 \text{ Pa}$$

$$k_{steel} = 0.495 \text{ m/s } (^\circ\text{C m}^2)^{-1}$$

$$\rho_{steel} = 0.281 \text{ kg/m}^3$$

$$C_{steel} = 1033 \text{ m/s } (^\circ\text{C})^{-1/2}$$

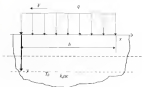


Figure 2.2 Moving head of heat sources on a semi-infinite solid

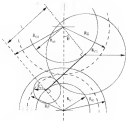


Figure 2.2: Mode of coverage of working with position

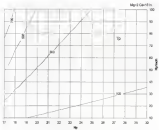


Figure 2.1 Temperature rise plot versus fuel and number of teeth for (C₁₂-10) as (Mg-10)

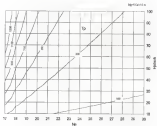


Figure 3.4 Temperature rise plot versus load and number of teeth for $(C_v = 0.05, \text{kg} = 1)$

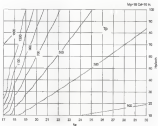


Figure 2-1 Temperature rise plot versus load and number of teeth for $(C_{10})_{10}$ in. (Fig. 10)

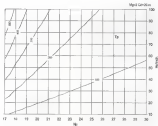


Figure 2.6 Temperature \log plot versus load and number of tests for $C_{50} = 20$ ms, $\log t = 0$.

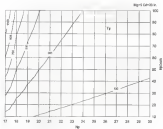
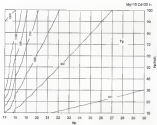


Figure 2.2 Composite size plot versus load and number of tests for $(C_{50})^{0.30}$ in (kg \cdot m)



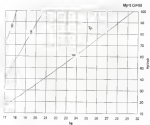


Figure 2-5 Temperature rise plot versus load and number of teeth for $(C_1=26 \text{ in, } b=1/2 \text{ in})$

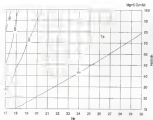


Figure 2.18 Tripenier's nom plot versus load and number of tests for $(C_{10}-3)/\alpha = 100$.

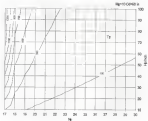


Figure 3.10.1 Temperature rise plot versus load and number of tests for $(C_{50})^{10}/a_{cr}$, (Eq. 10)

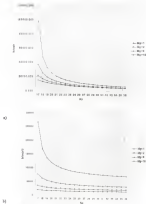
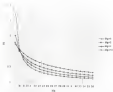
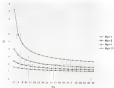


Figure 2.13 (a) Normal thermal stress and (b) Shear stress contact stress plots versus position and number of teeth for TC-20 m. Load ($W_d = 1000 \text{ N}$)



a)



b)

Figure 2-12 a) Dimensionless chemical and b) Dimensionless mechanical stress plots versus pore volume and number of weeks for ($C_{01}=20$ m., Load $(W_1)=1000$ lb.)

Table 2. Temperature rise values versus load and number of teeth for $PC_{20} = 50$ in. $h_{0.2} = 100$.

[illegible]

Table 2.10: Dependence important π -values (see) π -values and number of nodes for $K=70$ and $K=100$ (see) $K=100$

2010年 續前				
序號	單位名稱	單位地址	單位性質	備註
11	中國銀行	中國銀行總行	中央銀行	中國銀行總行
12	交通銀行	交通銀行總行	中央銀行	交通銀行總行
13	農業銀行	農業銀行總行	中央銀行	農業銀行總行
14	建設銀行	建設銀行總行	中央銀行	建設銀行總行
15	工商銀行	工商銀行總行	中央銀行	工商銀行總行
16	交通銀行	交通銀行總行	中央銀行	交通銀行總行
17	農業銀行	農業銀行總行	中央銀行	農業銀行總行
18	建設銀行	建設銀行總行	中央銀行	建設銀行總行
19	工商銀行	工商銀行總行	中央銀行	工商銀行總行
20	交通銀行	交通銀行總行	中央銀行	交通銀行總行
21	農業銀行	農業銀行總行	中央銀行	農業銀行總行
22	建設銀行	建設銀行總行	中央銀行	建設銀行總行
23	工商銀行	工商銀行總行	中央銀行	工商銀行總行
24	交通銀行	交通銀行總行	中央銀行	交通銀行總行
25	農業銀行	農業銀行總行	中央銀行	農業銀行總行
26	建設銀行	建設銀行總行	中央銀行	建設銀行總行
27	工商銀行	工商銀行總行	中央銀行	工商銀行總行
28	交通銀行	交通銀行總行	中央銀行	交通銀行總行
29	農業銀行	農業銀行總行	中央銀行	農業銀行總行
30	建設銀行	建設銀行總行	中央銀行	建設銀行總行
31	工商銀行	工商銀行總行	中央銀行	工商銀行總行
32	交通銀行	交通銀行總行	中央銀行	交通銀行總行
33	農業銀行	農業銀行總行	中央銀行	農業銀行總行
34	建設銀行	建設銀行總行	中央銀行	建設銀行總行
35	工商銀行	工商銀行總行	中央銀行	工商銀行總行
36	交通銀行	交通銀行總行	中央銀行	交通銀行總行
37	農業銀行	農業銀行總行	中央銀行	農業銀行總行
38	建設銀行	建設銀行總行	中央銀行	建設銀行總行
39	工商銀行	工商銀行總行	中央銀行	工商銀行總行
40	交通銀行	交通銀行總行	中央銀行	交通銀行總行
41	農業銀行	農業銀行總行	中央銀行	農業銀行總行
42	建設銀行	建設銀行總行	中央銀行	建設銀行總行
43	工商銀行	工商銀行總行	中央銀行	工商銀行總行
44	交通銀行	交通銀行總行	中央銀行	交通銀行總行
45	農業銀行	農業銀行總行	中央銀行	農業銀行總行
46	建設銀行	建設銀行總行	中央銀行	建設銀行總行
47	工商銀行	工商銀行總行	中央銀行	工商銀行總行
48	交通銀行	交通銀行總行	中央銀行	交通銀行總行
49	農業銀行	農業銀行總行	中央銀行	農業銀行總行
50	建設銀行	建設銀行總行	中央銀行	建設銀行總行

Table 1.11 Normal thermal stress values for temperature rise values, stress gear values and number of teeth for ($C_p=28$ in./in./ $^{\circ}\text{F}$), load ($W_d=1000$ lb.)

Normal Thermal Stress Values, σ_{Thermal} (psi)				
W_d	Stress	Stress	Stress	Stress
17	121100-1217	213300-1217	305500-1217	397700-1217
18	121100-1218	213300-1218	305500-1218	397700-1218
19	121100-1219	213300-1219	305500-1219	397700-1219
20	121100-1220	213300-1220	305500-1220	397700-1220
21	121100-1221	213300-1221	305500-1221	397700-1221
22	121100-1222	213300-1222	305500-1222	397700-1222
23	121100-1223	213300-1223	305500-1223	397700-1223
24	121100-1224	213300-1224	305500-1224	397700-1224
25	121100-1225	213300-1225	305500-1225	397700-1225
26	121100-1226	213300-1226	305500-1226	397700-1226
27	121100-1227	213300-1227	305500-1227	397700-1227
28	121100-1228	213300-1228	305500-1228	397700-1228
29	121100-1229	213300-1229	305500-1229	397700-1229
30	121100-1230	213300-1230	305500-1230	397700-1230
31	121100-1231	213300-1231	305500-1231	397700-1231
32	121100-1232	213300-1232	305500-1232	397700-1232
33	121100-1233	213300-1233	305500-1233	397700-1233
34	121100-1234	213300-1234	305500-1234	397700-1234
35	121100-1235	213300-1235	305500-1235	397700-1235
36	121100-1236	213300-1236	305500-1236	397700-1236
37	121100-1237	213300-1237	305500-1237	397700-1237
38	121100-1238	213300-1238	305500-1238	397700-1238
39	121100-1239	213300-1239	305500-1239	397700-1239
40	121100-1240	213300-1240	305500-1240	397700-1240

Table 1.12 Temperature mechanical stress values stress gear values and number of teeth for ($C_p=28$ in./in./ $^{\circ}\text{F}$), load ($W_d=1000$ lb.)

Temperature Mechanical Stress Values, σ_{Thermal} (psi)				
W_d	Stress	Stress	Stress	Stress
17	121100-1241	213300-1241	305500-1241	397700-1241
18	121100-1242	213300-1242	305500-1242	397700-1242
19	121100-1243	213300-1243	305500-1243	397700-1243
20	121100-1244	213300-1244	305500-1244	397700-1244
21	121100-1245	213300-1245	305500-1245	397700-1245
22	121100-1246	213300-1246	305500-1246	397700-1246
23	121100-1247	213300-1247	305500-1247	397700-1247
24	121100-1248	213300-1248	305500-1248	397700-1248
25	121100-1249	213300-1249	305500-1249	397700-1249
26	121100-1250	213300-1250	305500-1250	397700-1250
27	121100-1251	213300-1251	305500-1251	397700-1251
28	121100-1252	213300-1252	305500-1252	397700-1252
29	121100-1253	213300-1253	305500-1253	397700-1253
30	121100-1254	213300-1254	305500-1254	397700-1254
31	121100-1255	213300-1255	305500-1255	397700-1255
32	121100-1256	213300-1256	305500-1256	397700-1256
33	121100-1257	213300-1257	305500-1257	397700-1257
34	121100-1258	213300-1258	305500-1258	397700-1258
35	121100-1259	213300-1259	305500-1259	397700-1259
36	121100-1260	213300-1260	305500-1260	397700-1260
37	121100-1261	213300-1261	305500-1261	397700-1261
38	121100-1262	213300-1262	305500-1262	397700-1262
39	121100-1263	213300-1263	305500-1263	397700-1263
40	121100-1264	213300-1264	305500-1264	397700-1264

Table 2.63 Maximal meshwork contact stress values for transport case values versus gear ratios and number of teeth for $K_{H\beta}=20$, $\alpha=20^\circ$ Load ($F_{H\beta}=2000$ N)

Z	Z ₂ (gear) Number of teeth (Z ₁ = 20)			
	20	25	30	35
10	12018,17	11011,17	10411,17	10000,00
11	11818,17	10811,17	10211,17	9799,99
12	11618,17	10611,17	10011,17	9599,97
13	11418,17	10411,17	9811,17	9399,95
14	11218,17	10211,17	9611,17	9199,93
15	11018,17	10011,17	9411,17	8999,91
16	10818,17	9811,17	9211,17	8799,89
17	10618,17	9611,17	9011,17	8599,87
18	10418,17	9411,17	8811,17	8399,85
19	10218,17	9211,17	8611,17	8199,83
20	10018,17	9011,17	8411,17	7999,81
22	9618,17	8611,17	8011,17	7599,79
24	9218,17	8211,17	7611,17	7199,75
26	8818,17	7811,17	7211,17	6799,71
28	8418,17	7411,17	6811,17	6399,67
30	8018,17	7011,17	6411,17	5999,63
32	7618,17	6611,17	6011,17	5599,59
34	7218,17	6211,17	5611,17	5199,55
36	6818,17	5811,17	5211,17	4799,51
38	6418,17	5411,17	4811,17	4399,47
40	6018,17	5011,17	4411,17	3999,43
42	5618,17	4611,17	4011,17	3599,39
44	5218,17	4211,17	3611,17	3199,35
46	4818,17	3811,17	3211,17	2799,31
48	4418,17	3411,17	2811,17	2399,27
50	4018,17	3011,17	2411,17	1999,23
52	3618,17	2611,17	2011,17	1599,19
54	3218,17	2211,17	1611,17	1199,15
56	2818,17	1811,17	1211,17	799,11
58	2418,17	1411,17	811,17	399,07
60	2018,17	1011,17	411,17	-0,00
62	1618,17	611,17	0,00	-400,00
64	1218,17	211,17	-411,17	-800,00
66	818,17	-189,17	-811,17	-1200,00
68	418,17	-589,17	-1211,17	-1600,00
70	18,17	-989,17	-1611,17	-2000,00
72	-382,17	-1389,17	-2011,17	-2400,00
74	-782,17	-1789,17	-2411,17	-2800,00
76	-1182,17	-2189,17	-2811,17	-3200,00
78	-1582,17	-2589,17	-3211,17	-3600,00
80	-1982,17	-2989,17	-3611,17	-4000,00
82	-2382,17	-3389,17	-4011,17	-4400,00
84	-2782,17	-3789,17	-4411,17	-4800,00
86	-3182,17	-4189,17	-4811,17	-5200,00
88	-3582,17	-4589,17	-5211,17	-5600,00
90	-3982,17	-4989,17	-5611,17	-6000,00
92	-4382,17	-5389,17	-6011,17	-6400,00
94	-4782,17	-5789,17	-6411,17	-6800,00
96	-5182,17	-6189,17	-6811,17	-7200,00
98	-5582,17	-6589,17	-7211,17	-7600,00
100	-5982,17	-6989,17	-7611,17	-8000,00

CHAPTER 3 DIMENSIONLESS RELATIONSHIP FOR CONTACT STRESS MODIFICATION

Thermal Stress

Thermal stress is the stress arising from non-uniform temperature distribution. When the material is subjected to a temperature gradient, the material tends to expand more on the higher temperature and less on the lower temperature side of the temperature gradient [24]. Thermal deformation simply means that as the "thermal" energy (and temperature) of a material increases, so does the vibration of its atoms and molecules, and this increased vibration results in what can be considered a stretching of the molecular bonds—which causes the material to expand. A system of thermal stress and thermal strains may be introduced which are dependent on the shape of body and the temperature distribution.

The thermal stress equation as given in equation (2-11) and presented below is depend on material parameters such as modulus of elasticity (E), thermal expansion coefficient (α), poisson's ratio (ν), and the temperature gradient (ΔT)

$$\sigma_{xx} = \frac{E\alpha\Delta T}{(1-\nu_x)} \quad (3-1)$$

A linear relationship between the stress and strain within the elastic region is given by Hooke's law and represented by equation (3-2) as

$$\sigma_{xx} = E\varepsilon \quad (3-2)$$

where, ε = thermal strain.

Thermal Fatigue

Although brittle materials may fail in one cycle of thermal stress application, ductile materials may require one or more cycle of thermal stress before fracture is generated. Failure under repeated application of thermal stress is called *thermal stress fatigue*. Thermal fatigue is defined as the gradual deterioration and eventual cracking of material by alternate heating and cooling when first thermal expansion is possible or totally constrained [29].

The experimental studies showed that for the same plastic stress range, the number of cycles to failure were much less for thermally cycled specimens than mechanically-cycled specimens [29,30].

Low-Cycle Fatigue and High-Cycle Fatigue

Fracture fatigue investigation over the years resulted in the observation that the fatigue process actually consists of two domains of cyclic stressing or straining. One of the domains occurs in significant amounts of plastic stress resulted from high cyclic load and low number of cycles. This domain is commonly referred to as *low-cycle fatigue*. The other type is that the stress stays in the elastic range with low cyclic load and high number of cycle, which is referred to as *high-cycle fatigue*. The high-cycle fatigue range generally is defined as failure at 50000 cycles or above [31].

Generally, low-cycle thermal fatigue failures under high temperatures are observed as intergranular cracks and high cycle fatigue with moderate temperatures cycling are observed as transgranular cracks. For microcrystalline failure, fatigue cracks propagate through grain along slip bands or crystallographic planes. On the other hand,

intercrystalline cracking refers to separation along the boundaries between grains as a result of stresses and movement of the entire grain.[13]

Thermal Shock

When the thermal stress is generated by sudden changes in temperature, the problem is referred to as thermal shock. The stresses induced in thermal shock are often greater than those due to slow heating and cooling. The materials may be subjected by rapid application of stress and therefore may not be able to withstand the thermal shock.[14] Thermal shock stress is characterized as a severe stress field generated in a structure by sudden application of a large heat flux, which increases the surface temperature instantaneously.[15]

The thermal shock resistance of brittle materials is determined by the temperature rise that will cause failure in one load-cycle. The maximum shock temperature for failure is given using the single cycle resistance as

$$T_{max} = \frac{\sigma_{max}}{E\alpha} \quad (3.3-a)$$

for low values of β (brittle materials) (Bridgman theory), and

$$T_{max} = \frac{\sigma_b}{E\alpha} \quad (3.3-b)$$

for high values of β (ductile materials),

where σ_{max} = the maximum stress

σ_b = the breaking stress (fracture stress)

α = thermal expansion coefficient

E = modulus of elasticity

$\beta = \pi R^2 / L$, is the heat transfer modulus, a dimensionless heat transfer parameter, that depends on the viscosity η , thermal conductivity k , and the characteristic size of the body x . The implications of (3.3a) and (3.3.4) is that for large β the conductivity does not influence the temperature that can be tolerated without failure.

For ductile materials, failure occurs with multiple-cycles rather than being caused by a single application of load. The failure of ductile materials due to repeated thermal shock loading is given as [29]

$$N_f = G(\alpha \Delta T_c)^{-2} \epsilon_{tc}^2 \quad (3.4)$$

where G and d are constants

α = the thermal expansion coefficient, $1/^\circ\text{F}$

ΔT_c = change in temperature, $^\circ\text{F}$

ϵ_{tc} = the elastic limit of the material, psi

Endurance Limit

Most metals follow the characteristic pattern of failure occurring at an increasingly larger number of loading cycles when the stress is reduced. The endurance limit is the highest stress at which material can be subjected to repeated stress without failure. This value is obtained from a stress-number of cycles ($S-N$) diagram. Ferrous metals usually exhibit a characteristic limit in these plots, as shown in figure 3.1, and the endurance limit is the asymptote [34]. Moreover, some materials do not have well-defined limits. In this case usually, the fatigue limit at a high cyclic life ($> 10^7$ cycles) will also be called the endurance limit.

Combined Thermal and Mechanical Stress Effect on Fatigue

Thermal stress cycling coupled with the mechanical stresses developed at the asperity contact interaction cause cracks to appear early in the life of rolling-sliding contact steels [34].

Experimental studies for investigating the repeated thermal shock stress effects on bending fatigue of two types of high-carbon (A548-C90) and low-carbon (1020) steels are reported in reference [35]. The tests were done on standard specimens with and without thermal shock application. The results of the tests are given in Figures 3-2 to 3-3.

The results prove that high-carbon steel endurance limit is decreased 45% with 40 thermal cycles. For 1020 low-carbon steel endurance limit is also decreased but only 10%.

The above study shows the material life is dependent on the combined mechanical and thermal stresses when the component is under application of both loads [35].

Therefore, the following design criterion is applied in this study

$$I = \sqrt{\left(\frac{\sigma_m}{K_m \sigma_u}\right)^2 + \left(\frac{\sigma_t}{K_t \sigma_u}\right)^2} \quad (3.5)$$

where σ_m = the mechanical tensile stress on the surface

σ_t = the thermal tensile stress on the surface

σ_u = the ultimate tensile strength

K_m = the ratio of the fatigue limit due to mechanical loading to the ultimate tensile strength

K_t = the ratio of the thermal fatigue limit to the ultimate tensile strength

for the nominal and real area of contact

C_d = Corner distance

ω_r = angular velocity of pinion

AP = applied load (horse power)

The modification factors (K_f) and $\frac{1}{\sqrt{1+K}} = \left(\frac{K_{\text{sur}}}{K_{\text{sur}} + K} \right)$ are evaluated for gear ratios

2.5 and 10; corner distances 18, 30 and 50 in. and load 18 to 100 kip for the following data and conditions:

Steel data

$$E_{\text{steel}} = 30 \text{ kpsi}, \nu_{\text{steel}} = 0.31 \text{ (in}^2/\text{in}^2 \text{) (in/in)}^2$$

$$G_{\text{steel}} = 8.46 \text{ (in}^2/\text{in}^2 \text{) (in}^2/\text{in}^2 \text{)}, \rho_{\text{steel}} = 0.283 \text{ (lb/in}^3 \text{)}, \alpha_{\text{steel}} = 10.5 \text{ (in/in}^2 \text{) (in}^2/\text{in}^2 \text{)}$$

Gear materials

4340 high-carbon steel and 1020 low-carbon steel,

Ultimate strength of materials

Two cases are considered for determining the allowable ultimate stress

In the first case, the temperature effect on reducing the ultimate stress is not considered and the values used are as follows:

$$s_u \text{ (4340 high-carbon steel)} = 180 \text{ (ksi)}^2/\text{psi}$$

$$s_u \text{ (1020 low-carbon steel)} = 100 \text{ (ksi)}^2/\text{psi}$$

In the second case ultimate strength is considered to be affected by the temperature rise. The values of the ultimate strength in this case are given by figure 7-3.

Pinion rotational speed (ω_p) = 100 rad/sec., pressure angle (ϕ) = 20° , Lewis form coefficient, Y_F = 0.3, and the coefficient of friction (μ) = 0.05 are used in the calculations.

The results are given in tables 3-3 to 3-10 and plotted in figures 3-6 to 3-14 for the first case. The values show that the allowable mechanical stress is decreased with lower number of teeth, higher load and higher gear ratio as a result of the imposed thermal stress.

The next study in this research deals with the effect of the ultimate strength change with temperature. Therefore the ultimate strengths of the materials (3-16 high-carbon steel and 3-18 low-carbon steel) are modified for the temperatures as given in chapter 2.

Accordingly, the modification parameters can be expressed as

$$\frac{\sigma_{u_0}}{\sqrt{1+K}} = \left(\frac{\sigma_{u_0}}{K_u \sigma_{u_1}} \right) \quad (3-11)$$

where: σ_{u_0} = ultimate strength at the specific temperature

σ_{u_1} = ultimate strength at given temperature (without temperature change consideration).

The results given in tables 3-11 to 3-12 and plotted in figures 3-15 to 3-21 shows that with the higher temperature the allowable mechanical stress decreases further as a result of the decrease in ultimate strength.

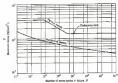


Figure 3.1 Typical endurance stress curves (S-N)

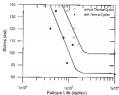


Figure 3.1: Fatigue data for A540 steel (High-carbon) [27]

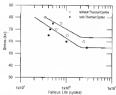


Figure 5.2 Fatigue data for 1050 low carbon steel [23]



Figure 3-3 Design approach plot

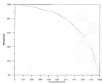


Figure 3-4 Ultimate strength design versus temperature plot

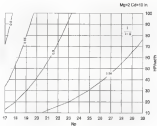


Figure 1-6 Design factor $q'/(1+K)$ versus load and number of teeth for $p_c = 13$ in.
 Mg=2

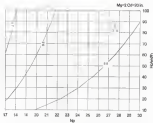


Figure 2.1 Design factor $K' \sqrt{1 + R_2}$ versus load ratio number of teeth for CC and 20mm.
 (Eq. 2.1)

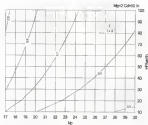


Figure 1-8 Design factor $k_p \sqrt{1 + R}$ versus total and number of levels for $(C_p)/500$ $k_p = 10$.

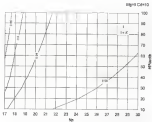


Figure C6-13 Design Factor $K_s \sqrt{1 + R_s}$ versus limit and number of tests for $(Z_{1-\alpha} + 1.64s_{\bar{y}})/\sigma_{\bar{y}} = 5$

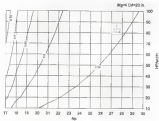


Figure 3-18 Change factor $j' / \sqrt{1 + A_j}$ versus load and number of teeth for $C_H = 25$ in. ($M_2 = 3$)

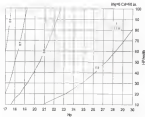


Figure 3-11 Design Factor $\frac{1}{\sqrt{1+K}}$ versus load and number of teeth for $(C_p=5000, \log=0)$

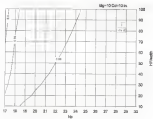


Figure 1-11 Design factor $K_t / \sqrt{1 + K}$ versus load and number of teeth for $Q_v = 15$ ft/min, 1000 psi.

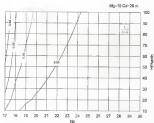


Figure 3-12 Design factor $K_s(1+K_s)$ versus load and number of teeth for $(C_p=280, \log=13)$.

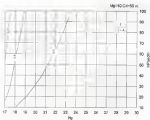


Figure 3.24: Design factor $1/\sqrt{1+R^2}$ versus load and number of teeth for QC-55a ($M_g=1$)

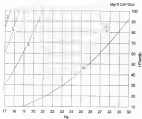


Figure 3-13 Design factor $\frac{R_p/R_c}{\sqrt{1+K_u}}$ versus load and number of bolts for $(C_u=10)$ at $M_y=0$.

$M_y=0$

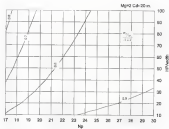


Figure 3.10- Design factor $\left(\frac{C_p \sigma_{ps} \sigma_{ps}}{\sigma_p^2 (1 + K_t)}\right)$ versus total seal number of teeth for $(C_p=25$ in.

$M_p=2$)

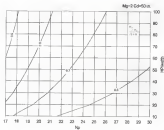
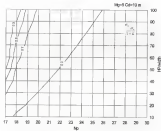


Figure 1.11 Design factor $\frac{F_m}{\sqrt{1+R_1}}$ versus load and number of teeth for $(C_D=50\text{ m.})$

$Mg=1)$



Example 8.23 Design factor $\left(\frac{\sigma_{Bn} \sigma_{Bt}}{\sigma_{Bn} \sigma_{Bt}}\right)$ versus load and number of teeth for $(C_d = 1.8 \text{ in.})$

$M_d = 0$

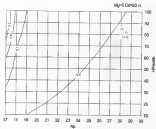


Figure J-18 Design factor $\frac{\sigma_y}{\sigma_x / \sqrt{1 + R}}$ versus load and number of tests for $R=0$.

$R=0$

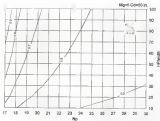


Figure 3-28 Design factor $\frac{C_{FS}(s_{FS})}{\sqrt{1+K}}$ versus load and number of teeth for $(C_F=10$ and $M_F=0)$

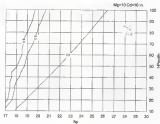


Figure 3-2 Design factor $\frac{(K_t S_u / S_e) S_n}{\sqrt{1 + K_t}}$ versus lead and number of teeth for $(C_d = 0.15)$.

$M_d = 100$

Fig-12 C=20 in

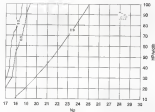


Figure 1-12 Design factor $\frac{S_A}{S_B} \left(\frac{S_A}{S_B} \right)$ versus load and number of teeth for $C=20$ in.

Fig-12

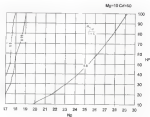


Figure 3-11 Design factor $\frac{F_d}{F_u}$ versus load and number of teeth for $(C_1=150 \text{ in.}, M_g=18)$.

Table 3.4 Factors K_L , K_S for condensed mechanical and thermal fatigue for 4340 high carbon steel and 1020 low carbon steel

4340 High carbon steel

σ^T : 1667	$(\sigma_b)^T$: 1140
σ^T : 1611 m/si ²	$(\sigma_b)^T$: 826 ksi
ν : 0.3	
E : 30×10^6 psi	

Number of cycle	10^3	10^4	10^5	10^6	10^7	10^8	10^9
$\sigma_{b,eq}$	140	128	116	105	100	90	80
$\sigma_{b,eq}$	111	100	90	80	80	70	60
$\sigma_{b,eq}$ ksi	11.961	10.960	10.102	11.766	10.841	11.141	10.641
$K_L = (\sigma_{b,eq})^2 / \sigma_b^2$	0.75	0.88	0.82	0.76	0.83	0.85	0.73
$K_S = (\sigma_{b,eq})^2 / \sigma_b^2$	0.6	0.78	0.73	0.78	0.6	0.6	0.6

1020 Low carbon steel

σ^T : 367	$(\sigma_b)^T$: 487 ksi
σ^T : 1411 m/si ²	$(\sigma_b)^T$: 688 ksi
ν : 0.3	
E : 30×10^6 psi	

Number of cycle	10^3	10^4	10^5	10^6	10^7	10^8	10^9
$\sigma_{b,eq}$	50	46	46	43	40	40	40
$\sigma_{b,eq}$	50	46	40	40	37	34	34
$\sigma_{b,eq}$ ksi	40.67	37.1	32.7	33	30	27	27
$K_L = (\sigma_{b,eq})^2 / \sigma_b^2$	0.76	0.74	0.7	0.66	0.62	0.63	0.63
$K_S = (\sigma_{b,eq})^2 / \sigma_b^2$	0.61	0.68	0.63	0.65	0.64	0.55	0.55

Table 3.1 Design factor $k'_f \sqrt{1 + R_f}$ versus load and number of teeth for $(C_1 = 1.0)$ in Eq. (3)

Table 3.1									
Table 3.1									
Table 3.1									
Table 3.1									
Table 3.1									
Table 3.1									
Table 3.1									
Table 3.1									
Table 3.1									
Table 3.1									
Table 3.1									
Table 3.1									
Table 3.1									
Table 3.1									
Table 3.1									
Table 3.1									
Table 3.1									
Table 3.1									
Table 3.1									
Table 3.1									
Table 3.1									
Table 3.1									
Table 3.1									
Table 3.1									
Table 3.1									
Table 3.1									
Table 3.1									
Table 3.1									
Table 3.1									
Table 3.1									
Table 3.1									
Table 3.1									
Table 3.1									
Table 3.1									
Table 3.1									
Table 3.1									
Table 3.1									
Table 3.1									
Table 3.1									
Table 3.1									
Table 3.1									
Table 3.1									
Table 3.1									
Table 3.1									
Table 3.1									
Table 3.1									
Table 3.1									
Table 3.1									
Table 3.1									
Table 3.1									
Table 3.1									
Table 3.1									
Table 3.1									
Table 3.1									
Table 3.1									
Table 3.1									
Table 3.1									
Table 3.1									
Table 3.1									
Table 3.1									
Table 3.1									
Table 3.1									
Table 3.1									
Table 3.1									
Table 3.1									
Table 3.1									
Table 3.1									
Table 3.1									
Table 3.1									
Table 3.1									
Table 3.1									
Table 3.1									
Table 3.1									
Table 3.1									
Table 3.1									
Table 3.1									
Table 3.1									
Table 3.1									
Table 3.1									
Table 3.1									
Table 3.1									
Table 3.1									
Table 3.1									
Table 3.1									
Table 3.1									
Table 3.1									
Table 3.1									
Table 3.1									
Table 3.1									
Table 3.1									
Table 3.1									
Table 3.1									
Table 3.1									
Table 3.1									
Table 3.1									
Table 3.1									
Table 3.1									
Table 3.1									
Table 3.1									
Table 3.1									
Table 3.1									
Table 3.1									
Table 3.1									
Table 3.1									
Table 3.1									
Table 3.1									
Table 3.1									
Table 3.1									
Table 3.1									
Table 3.1									
Table 3.1									
Table 3.1									
Table 3.1									
Table 3.1									
Table 3.1									
Table 3.1									
Table 3.1									
Table 3.1									
Table 3.1									
Table 3.1									
Table 3.1									
Table 3.1									
Table 3.1									
Table 3.1									
Table 3.1									
Table 3.1									
Table 3.1									
Table 3.1									
Table 3.1									
Table 3.1									
Table 3.1									
Table 3.1									
Table 3.1									
Table 3.1									
Table 3.1									
Table 3.1									
Table 3.1									
Table 3.1									
Table 3.1									
Table 3.1									
Table 3.1									
Table 3.1									
Table 3.1									
Table 3.1									
Table 3.1									
Table 3.1									
Table 3.1									
Table 3.1									
Table 3.1									
Table 3.1									
Table 3.1									
Table 3.1									
Table 3.1									
Table 3.1									
Table 3.1									
Table 3.1									
Table 3.1									
Table 3.1									
Table 3.1									
Table 3.1									
Table 3.1									
Table 3.1									
Table 3.1									
Table 3.1									
Table 3.1									
Table 3.1									
Table 3.1									
Table 3.1									
Table 3.1									
Table 3.1									
Table 3.1									
Table 3.1									
Table 3.1									
Table 3.1									
Table 3.1									
Table 3.1									
Table 3.1									
Table 3.1									
Table 3.1									
Table 3.1									
Table 3.1									
Table 3.1									
Table 3.1									
Table 3.1									
Table 3.1									
Table 3.1									
Table 3.1									
Table 3.1									
Table 3.1									
Table 3.1									
Table 3.1									
Table 3.1									
Table 3.1									
Table 3.1									
Table 3.1									
Table 3.1									
Table 3.1									
Table 3.1									
Table 3.1									
Table 3.1									
Table 3.1									
Table 3.1									
Table 3.1									
Table 3.1									
Table 3.1									
Table 3.1									
Table 3.1									
Table 3.1									
Table 3.1									
Table 3.1									
Table 3.1									
Table 3.1									
Table 3.1									
Table 3.1									
Table 3.1									
Table 3.1									
Table 3.1									
Table 3.1									
Table 3.1									
Table 3.1									
Table 3.1									
Table 3.1									
Table 3.1									
Table 3.1									
Table 3.1									
Table 3.1									
Table 3.1									
Table 3.1									
Table 3.1									
Table 3.1									
Table 3.1									
Table 3.1									
Table 3.1									
Table 3.1									
Table 3.1									
Table 3.1									
Table 3.1									
Table 3.1									
Table 3.1									
Table 3.1									
Table 3.1									
Table 3.1									
Table 3.1									
Table 3.1									
Table 3.1									
Table 3.1									
Table 3.1									
Table 3.1									
Table 3.1									
Table 3.1									
Table 3.1									
Table 3.1									
Table 3.1									
Table 3.1									
Table 3.1									
Table 3.1									
Table 3.1									
Table 3.1									
Table 3.1									
Table 3.1									
Table 3.1									
Table 3.1									
Table 3.1									
Table 3.1									
Table 3.1									
Table 3.1									
Table 3.1									
Table 3.1									
Table 3.1									
Table 3.1									
Table 3.1									
Table 3.1									
Table 3.1									
Table 3.1									
Table 3.1									
Table 3.1									
Table 3.1									
Table 3.1									
Table 3.1									
Table 3.1									
Table 3.1									
Table 3.1									
Table 3.1									
Table 3.1									
Table 3.1									
Table 3.1									
Table 3.1									
Table 3.1									
Table 3.1									
Table 3.1									
Table 3.1									
Table 3.1									
Table 3.1									
Table 3.1									
Table 3.1									
Table 3.1									
Table 3.1									
Table 3.1									
Table 3.1									
Table 3.1									
Table 3.1									
Table 3.1									
Table 3.1									
Table 3.1									
Table 3.1									
Table 3.1									
Table 3.1									

Table 3-18 Design factor $\frac{(S_u - S_m)}{S_u}$ versus load and number of teeth for (C₁ = 100 in.

Fig-18)

		$\frac{S_u}{S_m}$		if stress concentration due to stress peak structure		Fig-17 C ₁ = 100			
		$\frac{S_u}{S_m}$							

CHAPTER 4 INVESTIGATION OF THE EFFECT OF SURFACE ROUGHNESS AND LUBRICATION ON MAXIMUM TEMPERATURE IN THE CONTACT ZONE

Lubricated Film

When two clean surfaces slide with no lubricant between them (dry conditions) the friction force at the interface decreases slightly with sliding speed and is independent of contact area[27]. The friction coefficient increases with the applied normal load on the surfaces and is dependent on the physical nature of the surfaces.

Sliding surfaces can be separated by a lubricant film so that there will be no direct contact between surfaces. Under such conditions the physical characteristics of the surfaces are insignificant for the friction. In this case, the friction coefficient is independent of load, and is generally proportional to the speed and the viscosity of the lubricant, and inversely proportional to the thickness of the lubricant film. When the lubricant film thickness is of the same dimension as the surface roughness the laws of hydrodynamics no longer apply. This case is called boundary friction, which can be the result of heavy load, starting from rest, slow sliding speed, and reversal of sliding direction.

For lightly loaded lubricated cylindrical contacts, the film thickness is affected by the elastic deformation of the material. This requires the use of elastohydrodynamic lubrication. Under such conditions with the assumption of smooth surfaces without asperities, a simplified film thickness equation is given by Dowson and Higginson, [34],

$$h = 2 \times 10^{-8} \sqrt{\mu_0 P / \dot{E}_0} \quad (4.1)$$

$$\text{where } P_0 = \frac{P_1 + P_2}{2}, \text{ is rolling velocity} \quad (4.2)$$

$$P = \mu_0 \dot{E}_0$$

$$P_1 = \mu_0 \dot{E}_1 \text{ is the surface velocity, [m/sec] or [cm/sec]} \quad (4.3)$$

$$\dot{E}_0 = \frac{E_1 E_2}{E_1 + E_2} \text{ is effective strain, [m] or [cm]} \quad (4.4)$$

$$\text{and } \mu_0 \text{ is the lubricant viscosity at the inlet temperature, poise = g/cm² sec (cgs)}$$

The maximum hydrodynamic lubrication film thickness for compressible, isothermal, smooth, unlubricated and fully flexible cylinders by a Newtonian lubricant is given by Hamrock and Jacobson in a dimensionless form [26] as

$$\frac{h}{E_0} = 2.35 \left[\frac{E_1 E_2}{E_0 E_0} \right]^{0.7} \left[\mu_0 \dot{E}_0 \right]^{-0.7} \left[\frac{P_1}{E_1 E_0} \right]^{-0.7} \quad (4.5)$$

where

$$\frac{h}{E_0} \text{ dimensionless film thickness parameter}$$

$$\frac{E_1 E_2}{E_0 E_0} \text{ dimensionless speed parameter}$$

$$\mu_0 \dot{E}_0 \text{ dimensionless materials parameter}$$

$$\frac{P_1}{E_1 E_0} \text{ dimensionless load parameter and } \alpha_1 \text{ is the pressure viscosity coefficient}$$

of the lubricant and μ_0 is the lubricant inlet temperature. The effect of pressure on

viscosity can be expressed as $\mu = \mu_0 e^{\alpha_1 P}$ where μ is the viscosity at a given pressure P

The lubricant viscosity is highly influenced by the temperature. Accordingly, the thermal effect due to the generated heat on the lubricant should be considered when calculating the lubricant film thickness. A correction factor, which is defined as a ratio of the thermal film thickness to that predicted by isothermal theory (IT) can be given as

$$CCF = \frac{1}{1 + \left(\frac{P}{2000} \right) + (34.42)^{-0.7} \lambda^{0.14}} \quad (4.6)$$

$$\text{where } \lambda = \frac{(T_f - T_c)}{(T_c + T_f)} \text{ is slide-to-roll ratio} \quad (4.7a)$$

$$\lambda = \frac{\mu_s \beta^{0.7}}{k_s} \text{ is thermal loading parameter} \quad (4.7b)$$

β the lubricant temperature-viscosity coefficient, based on the viscosity model
 k_s the lubricant thermal conductivity, then the dynamic viscosity including the thermal effect becomes,

$$\mu = \mu_{ref} \exp \left(\mu_s P - \beta (T - T_{ref}) \right) \quad (4.7c)$$

The dimensionless film thickness, which is a function of the slide-to-roll ratio (λ) and the thermal loading parameter (λ), is therefore given as

$$\left(\frac{h}{R_s} \right)_{\text{corr}} = CCF \left(\frac{h}{R_s} \right)_{\text{isothermal}} \quad (4.8)$$

The thermal loading parameter can be negligible for low loading speeds ($\lambda < 0.1$). However, for high speeds or high viscosity lubricants it can lead to a substantial change in film thickness.

4.1.3.1.1.1. Friction and Surface Roughness

The surface of metal bodies is not ideally smooth. In machining engineering materials, surface roughness is created. Surface roughness plays an important role in

machines design. During a metal cutting operation, a machined surface is created as a result of the movement of the tool edge relative to the work piece. Although various factors affect the surface roughness, it is generally accepted that the cutting parameters such as speed, feed rate, depth of cut and tool nose radius have significant influence on the surface geometry. The surface roughness increases with increasing machine tool stiffness, cutting speed, and tool nose radius, and decreasing feed rate [36-40].

Some other studies indicated that tool wear causes the surface finish to deteriorate rapidly and has a direct effect on the maximum roughness [41]. Based on an extensive experimental study using a ball, Hasegawa et al. [42] developed a statistical relationship of peak to valley surface roughness, R_{max} , in terms of cutting speed, feed rate, depth of cut, and tool nose radius using a response-surface method. The statistical relationship is given as

$$R_{max} = 0.25V^{-0.45}f^{0.15}d^{0.45}r^{-0.05} \quad (48)$$

where V = cutting speed

f = feed rate

d = tool radius

r = depth of cut

A parametric dynamic solution of the interaction between the tool and work piece system in turning is reported by Jung and Fray [43]. A generalized computer-based model is developed for predicting surface roughness for any given constant wheel speed, with consideration of the important parameters influencing deterministic vibratory behavior of the machine tool-work piece system. The parameters considered under investigation are the feed rate, cutting speed, depth of cut, radius of the cutting edge, the

dimensions of the work piece and the tool, stiffness, and the damping of the machine structure as well as the cutting tool assembly. They have validated the simulation to develop generalized equations for surface roughness based on output from the vibratory model. A generalized equation of the following form is developed

$$R_{\text{max}} = C' V^{0.2} f^{0.75} a^{0.75} r^{0.4} \quad (4.13)$$

The results as generated from the simulation for cutting conditions covering the practical range of applications are used in a regression analysis to obtain the best fit for the equation parameters C' , k_1 , k_2 , k_3 and k_4 .

All the simulated results were curve-fitted to give the following equations

$$C' = 7.05(2.25) \times 10^{-16} e^{0.0001 k_1}$$

$$k_1 = -0.27(23) + 0.311(23) \times e^{0.0001 k_2}$$

$$k_2 = 0.46(22) + 1.26(26) \times e^{0.0001 k_3}$$

$$k_3 = 0.34(29) + 0.62(31) \times e^{0.0001 k_4}$$

$$k_4 = -0.047(56) + 0.032(57) \times 10^{-0.0001 k_5}$$

where $\omega = \omega_n$ natural frequency of tool assembly (Hz)

These equations are applicable for the following conditions

$$R_p > 0.0015 \text{ mm}$$

$$0.1 \text{ mm/min} < V < 200 \text{ mm/min}$$

$$0.125 \text{ mm/min} < f < 0.50 \text{ mm/min}$$

$$0.10 \text{ mm} < a < 0.75$$

$$0.75 \text{ mm} < r < 2.50$$

The Contact between Rough Surfaces

When rough surfaces come into contact the contact is discrete (figure 4-1). The sum of these discrete contact areas forms the real contact area. The real contact area defines those parts of the surfaces where there is direct interaction between the bodies and determines the dimensions of the film space in lubricated bearing. The surface *deformation* or *strain* during sliding is also closely related to the size of the real contact area since the most stressed material near the surface are deformed by the real contact dimensions. Formation of the real contact area under load occurs as a result of the interpenetration or compressive deformation of individual asperities.

Hertz's solution [189] of the contact problem based on elasticity theory is widely used in calculating the real contact area for smooth solids. For the case of spherical surfaces, the contact area (A_c) changes with the load N according to the following relationship

$$A_c \propto N^{2/3} \quad (4-11)$$

In 1934 Bowden and Tabor [41] established that the real area of contact is directly proportional to load. They subsequently assumed that all real contacts are in the plastic state. Archard [44-46] calculated a whole range of "realistic" models for "spheres in spheres" and reached the conclusion based on elastic deformation that the real contact area follows the approximate relation

$$A_c \propto N^{3/4} \quad (4-12)$$

In this model, newly formed contact points account for the increase of real contact area with an increase in load more than the increase in size of the existing contact points.

The Greenwood-Williamson surface model [40] treats the contact of two rough elastic surfaces as the contact of equivalent-elastic rough surface and smooth elastic plane. This model is used to calculate the real area of contact for the rough surfaces. The rough surface is assumed to be covered with asperities whose summits are of spherical in shape and with constant asperity radius (R). The summit heights are randomly variable and uniformly distributed over a rough surface with a known density (λ_{sum}) [summits per unit area]. The mean height of the summits lies above the mean height of the surface as a whole by the amount (μ). The summit heights (z) are assumed to follow a normal or gaussian distribution with standard deviation (σ_z). The summit height distribution is assumed to be symmetrical about the mean summit height. This model contains three parameters, i.e.

- a) (R), the constant asperity radius
- b) (σ_z) the standard deviation of the summit heights
- c) (λ_{sum}), the number of summits per unit area.

A method of determining the values of these parameters of the Greenwood-Williamson surface roughness model is discussed by McCool's reference [45] with the following simplifications

- a) Summits on surfaces have the same height and curvature at peaks on profiles (e.g. measurements made along one arbitrary direction).
- b) The number of summits per unit area is the square of the linear density of peaks along one direction.
- c) The peak mean-plane contributed by the average height of profile peaks in a certain direction is the same as the summit mean surface

The root-mean-square height (R_q) and slope (R_{sq}) of a profile, obtainable as output of a profile measuring instrument, are used to determine the three parameters (k , r_0 , δr_{max}) needed for implementing the Greenwood-Williamson model for an asperity or equivalent envelope surface. Figure 4-1 shows that a smooth surface whose height above the nominal mean plane is z is situated at a distance $[z - \delta r - r_0]$ above the profile mean plane. The ratio $(R/R_q) = (\delta r/r_{max})$, often called the lateral film parameter (also referred to as the specific film thickness, λ) is found to be linearly related to (z/r_0) . For a specified $(\delta r/r_{max})$ value given the roughness and profile data of the surface, the dimensionless separation (z/r_0) and therefore the mean contact conditions at that time can be determined by using a Greenwood-Williamson model.

Thus, the area of contact sites for different load and speed conditions is calculated using the following equation

$$\frac{dA_c}{dx} = \pi R_{sq} dx \cdot f\left(\frac{z}{r_0}\right) \quad (4.11)$$

where A_c and dx are the real contact area and the nominal contact area respectively, $[m^2]$

$$f\left(\frac{z}{r_0}\right) = \left[1 - \left(\frac{z'}{z_0}\right)\left(x - \frac{z'}{z_0}\right)\right]^{1/2} \exp\left\{-\frac{1}{2}\left(\frac{z}{z_0}\right)^2\right\}$$

Coefficient of Friction of Lateral Sliding/Tilting Contact

There are many published empirical formulas for evaluating the coefficient of friction, which were developed by different investigators under different experimental conditions. Therefore they may not correlate with each other. All of these formulas are developed from test data in the thermal regime. Contacted empirical formulas are presented in these sliding/rolling conditions, which can then be used to construct the curve curve as illustrated in figure 4-3. The first point is μ_L , which gives the magnitude of

the rolling coefficient of friction. The second point is δ_0 , which gives the peak value of the coefficient of friction in the nonlinear region, which occurs at a sliding/rolling ratio between 0.05 & 0.27 (0.1 & 0.27). This point is also assumed to approximately define the end of the nonlinear region. The third condition is the thermal coefficient of friction, μ_t , after which the coefficient of friction is assumed to be almost independent of the sliding/rolling ratio. In this chapter our interest is going to focus on the thermal coefficient of friction because of the high sliding/rolling ratios, which are expected at the bottom of the tooth surface where damage generally occurs.

In the thermal regime, where the sliding/rolling ratio > 0.27, the coefficient of friction can be expressed as [27]

$$f = f_1 + (a_1 - a^2) R^2 \quad (4.10)$$

where f_1 is the coefficient of friction at $\delta_0 = 0$ from Figure 4-4

$$a = 0.2864 + 0.375 \times 10^{-4} \left(\frac{S_{fz}}{R_{fz}} \right) \\ a_1 = \frac{k_1}{1.875 \left(\frac{S_{fz}}{R_{fz}} \right) - 2.162 \times 10^{-4}} \quad (4.11)$$

where R_{fz} is the effective surface roughness from Figure 4-4

$\left(\frac{S_{fz}}{R_{fz}} \right)$ is the effective surface ratio, from Figure 4-4

R is effective radius

k_1 is the oil film thickness as calculated by Derwent Huggerton formula given in equation 4.1

The term h_f / K in equation (4.13) represents the influence of the lubricant film. The term (L_c / K) , represents the influence of the surface condition resulting from a particular manufacturing process.

Temperature Rise Calculations in Lubricated Rough Surface Contact

In this study, the temperature rise on the bulk surface and the segment are calculated based on whether the rise resulted from frictional heat input or viscous heat generation.

The considered lubrication conditions are given as below

The bulk surface is always covered by the lubricant. Therefore, the temperature rise is calculated based on viscous heating

The segment temperature rise is calculated based on frictional heating when the lubrication parameter $\lambda = \frac{h}{\sigma \sqrt{a_{eq}}} < 1.4$ implies some segment interaction.

The segment temperature rise is calculated based on viscous heating when lubrication parameter $\lambda = \frac{h}{\sigma \sqrt{a_{eq}}} > 1.4$ implies negligible segment interaction

where, h is lubricant film thickness

σ_{eq} is equivalent root mean square height

Temperature Rise Calculations Based on Frictional Heating

The temperature rise based on frictional heat input is given by equation (2.9) and involves below contains four different parameter groups

Material parameters $\phi_1 (v, \mu, E, K, \alpha, \dots)$

Geometric parameters $\phi_2 (M_p, N, \phi, a, \dots)$

Lubricant and surface parameters $\phi_3 (p, f, A_0, A_1, \dots)$

Application parameters $(\mu, \beta, \alpha, C_1, C_2)$

$$dV_2 = \pi R_2^2 (r_2 \mu, R_2, h, d) \pi R_2 (M_2, M_1) d_2 \mu_2 \pi d_2 \mu_2 f_2 d_2 \mu_2 d_2 dV_2 = \alpha \mu, C_1, C_2) \quad (4.16)$$

$$M_2 = \frac{1}{2\pi} \left[\frac{1}{\left[\frac{1-\alpha_2^2}{\alpha_2^2} + \frac{1-\alpha_1^2}{\alpha_1^2} \right]^{1/2}} \frac{1}{\beta \alpha_2} \right] \left[\frac{(1-\alpha_2)^2 \alpha_2^2 - (1-\alpha_1)^2 \alpha_1^2}{\alpha_2 \alpha_1^2 (1-\alpha_2)^2} \frac{\alpha_1^2}{\alpha_2^2} \right] d_2 \frac{d}{d_2} \left(\frac{dV_2}{\alpha_2^2 C_2 \mu_2} \right) \quad (4.17)$$

In this chapter, the lubrication and the surface roughness parameters for the main lines considered. These parameters are a function of coefficient of friction f , Ratio of nominal area of contact to real area of contact (A_n/A_r) and these parameter of coefficient μ .

The coefficient of friction is calculated by the procedure following the equation (4.14) and the ratio of nominal area to real area is calculated from Greenwood's

Williamson model

Temperature Rise Calculation Based on viscous Heating

Temperature rise due to viscous heating is analyzed using the procedure developed by Flad and Jurek, which is given in reference [3,4]. The model given in figure 4-7 is utilized to find the dimensionless temperature rise equations. The model represents two rolling/sliding cylinders having different radii, thermal properties and bulk temperatures, which are separated by a lubricant film with thickness h . The heat generation zone with thickness σ represents the liquid region where the lubricant undergoes a high shear rate. At moderate to high sliding speeds, the magnitude of σ is assumed to be approximately 0.1*h*. In order to simplify the derivation of the dimensionless equation for this case, σ is initially assumed to be equal to zero. Then the equations are given in [26].

$$\frac{T_{01} - T_{02}}{w} = \frac{1.04}{k_1} \left(\frac{T_{01} \rho_1 V_1^2}{2k_1} \right)^{0.5} \left(\frac{2k_1}{b} \right)^{-0.5} \left(\frac{k_1}{k_2} \right)^{-0.5} \int_0^{\max \left(\frac{1}{2} \frac{w}{k_1}, \frac{w}{k_2} \right)} \quad (4.18)$$

$$\text{and} \quad \frac{T_{01} - T_{02}}{w} = \frac{1.04}{k_1} \left(\frac{\rho_1 V_1^2 b}{k_1} \right)^{0.5} \quad (4.19)$$

where T_{01} is the maximum fluid film temperature

T_{02} is the minimum surface temperature

T_{01} is the bulk temperature

w is the heat partition coefficient (assumed to 5)

V_1 is the roller speed

ρ_1 and ρ_2 are the densities of gear material and fluid

c_1 and c_2 are the specific heats of material and fluid

k_1 and k_2 are the conductive heat transfer coefficient of material and the fluid

b is the film thickness

L is the contact width

The maximum heat input q per unit contact length is calculated from these terms S

$$q = V_1 k S \quad (4.20)$$

where V_1 is the sliding velocity and S is the shear stress can be calculated approximately

as

$$S = \mu \frac{V}{b} \quad (4.21)$$

Application to Gears

The applications in this study are considering two extreme conditions for the viscosity. In the first, the viscosity is assumed to be constant at the inlet temperature and in the second, the viscosity is assumed to be constant at the maximum surface

temperatures. Two different surface manufacturing processes, flat and the rough ground, are also considered. The properties of lubricant (oil: M) and the materials used are given in table 4-1.

The calculations are done for load 18 Np, gear mesh 2.5 and 10, the number of teeth A_p between 17 to 30 and contact distance $C_p(0)$ as

4.2. Numerical Results

Case 1 Temperature rise is calculated for flat ground gears with the assumption of constant oil viscosity corresponding to an inlet temperature (30 °C). The results are given in tables 4-4 to 4-6.

Case 2 Temperature rise is calculated for rough ground gears with the assumption of constant oil viscosity corresponding to an inlet temperature (30 °C). The results are given in tables 4-7 to 4-9.

Case 3 Temperature rise is calculated for flat ground gears with the assumption of constant oil viscosity corresponding to the maximum bulk surface temperature. The results are given in tables 4-10 to 4-12.

Case 4 Temperature rise is calculated for rough ground gears with the assumption of constant oil viscosity corresponding to the maximum bulk surface temperature. The results are given in tables 4-13 to 4-15.

The viscosity temperature relationship used is given by the following equation:

$$\mu(T) = \mu_0 e^{-\beta T} \quad (4.12)$$

where β is constant (for oil $\beta = 1.26 \times 10^{-4} \text{ } ^\circ\text{C}^{-1}$)

T is the temperature (°C)

μ_0 is constant which is equal to 70 Pa.s

$$p_0 = \text{atmospheric reference pressure } (p_0 = 1.4 \times 10^5 \text{ N/m}^2)$$

In case 2, instead of the viscosity and the surface temperature listed by standard as illustrated in the flow chart in figure 4-6

The results show that the temperature rise increases with the decrease of the number of teeth and the increase of the gear ratio. All the temperature calculations resulting from viscous shear input are based on the two extreme assumptions of oil film viscosity either as the inlet temperature or as the maximum surface temperature. Some of the temperature-rise values calculated based on these assumptions are extremely high and should be considered only as representation of trends. More realistic calculations of shear heating have to take into consideration the change in the viscosity and other oil properties gradually with temperature and pressure within the contact zone. This consideration requires very intensive computations and is beyond the scope of this study.

From this investigation it can be stated that the temperature rises on the surface and on the separator are comparable between the calculated temperatures based on the assumed extreme conditions.

The temperature rise based on viscous shear heat input is considered to be independent of the load applied. Further calculations are done specifically for the temperature rise on the separator for fine and rough ground gears subjected to loads between 10 to 100 lbf and gear ratios of 3 and 18 respectively. The results of the calculations are given in table 4-8 to 4-10. The results show that the temperature rise is highly affected by the increase of gear ratio and decrease of number of teeth for the shear heat input case and also affected by load for the frictional heat input case. The surface roughness also affects the temperature rise indirectly. Fine ground gears are generally

subjected to viscous heat input, which reduces the temperature rise at the asperities. Rough ground gears are generally subjected to decreased heat input due to the higher asperity height. Accordingly, the asperity temperature at the rough ground surface is generally higher than the fine ground surface although the bulk surface temperatures are same.

Contact Stress Modification Factor at Lubricated Rolling/Sliding Contact

The same approach given in chapter 3 for contact stress modification is applied in this chapter using the temperature rise calculated in section 4.4 for the asperities in the lubricated condition. The modification factors are calculated by using the equation (3.7) for high carbon steel (5240) and low-carbon steel (J 820) gears with rough and fine ground surfaces. As in the case of the temperature rise calculations for viscosity of the oil film is based on both the inlet temperature maximum surface temperature assumption.

The results of the contact stress modification factors, K , are given in tables 4-24

to 4-29. The parameter $\frac{1}{\sqrt{1+K}} = \left(\frac{\sigma_{H0}}{\sigma_{H0}'} \right)$ which represents the mechanical component of the total allowable stress for a given number of cycles under the combined thermal and mechanical loading is also calculated and the results are given in tables 4-30 to 4-32 and plotted in figures 4-16 to 4-18 for viscosity based on inlet temperature and tables 4-33 to 4-35 figures 4-19 to 4-21 for viscosity based on maximum surface temperature.

The results show that high carbon steel gears are significantly more affected by the thermal stress than low carbon steel gears. Increasing the load also increases the effect of thermal stress. Decreasing the number of teeth increases the effect of thermal stress. Fine ground gears are less influenced by thermal stress than rough ground gears.



Figure 5.1 Rough surfaces in contact

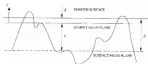


Figure 5.2 Contact of a rough surface and smooth plane

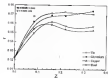


Figure 4.2 Variation of coefficient of friction with slenderness ratio, $V_0 = 0.383$ where [37]

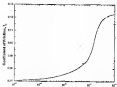


Figure 4.3 Coefficient of friction at $k_0/k_0 = 0$ against normalized Z_0/A [37]

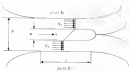


Figure 3.22 Lubricated, heavily loaded sliding/trailing cylinder [26]

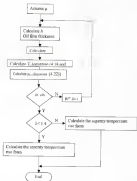
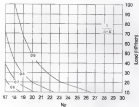


Figure 14 Flow chart of temperature rise calculations when viscosity constant at maximum surface



Example 3.11 Design Stress $S'_{\sqrt{1-K}}$ versus number of teeth and load for length ground and 4040 high-carbon steel gear, gear ratio 10:1, inside clearance 1.4-1.6 and constant of viscosity of oil temperature



Figure 4-10 Design factor $K_s \sqrt{1 + K}$ versus number of teeth and load for rough ground and 40-HRC-high carbon steel gears, gear ratio 10, center distance 10 and constant oil viscosity at inlet temperature

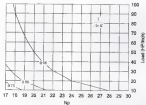


Figure 4.11. Design Factor $\left(\frac{S}{F}\sqrt{1+K}\right)$ versus number of teeth and load for 4340 steel gear and 4340 high carbon steel gear (gear ratio 40:1, center distance 100 mm and constant of elasticity in steel 200,000 MPa).

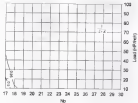


Figure 6.12 Design Factor $\frac{1}{\sqrt{1+K}}$ versus number of teeth and load for fine ground and 4140 high carbon steel gear (gear stress 54 kg/cm^2 , contact distance $Cd=1.0$ and constant oil viscosity at inlet temperature)

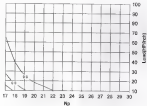


FIGURE 4-11 Design factor $1/\sqrt{1+K}$ versus number of teeth and load for rough ground and 100% low carbon steel gear pair and a 50% L, versus distance $CD=0$ and constant oil viscosity at 150 cP temperature

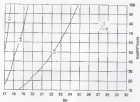


Figure 4-28 Design factor $Y' (\sqrt{1+K})$ versus number of teeth and load for rough ground steel (S20 low-carbon steel), gear ratio $M_G = 10$, center distance $C_d = 10$ and constant oil viscosity at inlet temperature.

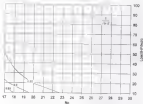


Figure 8.12 Design factor $K' \sqrt{F/F'}$ versus number of teeth and load for fine ground and 1050 low carbon steel gear, gear mesh $M_g = 2$, water distance $C_d = 18$ and constant oil viscosity at inlet temperature

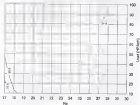


Figure 4.26 Design factor $\gamma_f/(1 + \bar{K})$ versus number of bolts and load for flat ground and 1020 low-carbon steel gusset plate: $M_d = 10$, ocean distance: $C_d = 10$ and constant oil viscosity at inlet temperature.

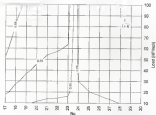


Figure 9.12 Design factor $K_s' \sqrt{1 + K_s}$ versus number of teeth and load for rough ground and 1040-high carbon steel gear (gear ratio 30:1, center distance 10–30 and constant oil viscosity at maximum surface temperature)

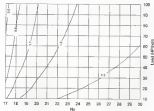


Figure 4-18 Design factor $\sqrt{Y_1 + A_2}$ versus number of teeth and load for rough ground and 4140 high carbon steel pins, gear ratio $M_2 = 10$, stress distance $C_1 = 10$ and constant oil viscosity at maximum surface temperature

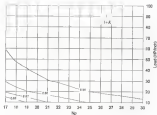


Figure 9-12 Design factor $\frac{1}{\sqrt{1+K}}$ versus number of teeth and load for Case ground and 6250-steel carbon steel gear: gear ratio $R_g=2$; stress-factor $C_s=1.0$ and constant oil viscosity of maximum surface temperature

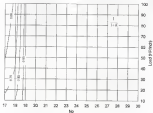


Figure 4-20 Damage factor $q^{1/4} \sqrt{1 + K}$ versus number of teeth and load for fair ground and 4140 high carbon steel gear—gear ratio 10:1—center distance C.D. 10 and constant oil viscosity at maximum surface temperature

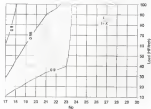


Figure 4-21. Design stress $S_g \sqrt{1+Z}$ versus number of teeth and load for rough ground and 1425-1600 low carbon steel gear with gear ratio 1.5, center distance 120-130 and minimum oil viscosity at maximum surface temperature.

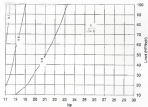


Figure 8-22 Design factor $K_t \sqrt{1 + K_f}$ versus number of teeth and load for rough ground and 132C45 carbon steel gear: gear ratio 14.4; center distance 12.5 in; constant oil viscosity at maximum surface temperatures.

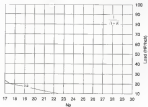


Figure 4.22 Design factor $K_d^1/\sqrt{1+K}$ versus number of teeth and load for fine ground and 133C-class carbon steel gear (gear ratio $m_g=2$, center distance $C/d=10$ and constant oil viscosity at entrance surface temperature)

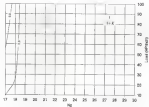


Figure 9-38 Design factor $Y_T \sqrt{1 + E}$ versus number of teeth and load for fine ground and 14.25 size carbon steel gear: gear ratio $m_g = 1.5$, center distance $C_d = 10$ and constant oil viscosity at ambient surface temperature

Table 4-1 Roughness and profile data for typical finishing operations

Surface Type	$R_{a, \mu\text{in}}$	λ/μ
Face Ground	2.54	0.04-0.7
Knurl Ground	21.5	0.0002
Lapped	2.54	0.0025
Polished	1.78	0.0115
Shot Peened	45.7	0.079

Table 4-2 Greenwood-Williamson model input parameters calculated for surface roughness data given in Table 4-1

Surface type	σ (standard deviation)	δ (μm) (asperity radius)	α , ($\mu\text{m/gal}$) (curvature factor)	$R_{q, \mu\text{m}}$ (quadrant-meanline) ²
Face Ground	21.5 (μ)	8.11	8.08 ⁻³	1.26 (μ)
Knurl Ground	12.8 (μ)	5.44	8.75	2.75 (μ)
Lapped	11 (μ)	4.74	8.74	1.86 (μ)
Polished	34.8 (μ)	9.12	8.88	2.88 (μ)
Shot Peened	21.2 (μ)	2.84	1.62	2.11 (μ)

Table 4.3 Lubricating oil and associated thermal and mechanical properties

Oil specifications

η_0 (mPa·sec)	η' (Pa·s)
100	50

Material (mechanical) properties (steel)

E (Pa)	E_c (Pa)	ν
207×10^9	1.7×10^9	0.3

Material (thermal) properties

α		C_p		ρ
(W/m·K) (oil)	(W/m·K) (steel)	(J/kg·K)	(J/kg·K)	(kg/m ³)
0.14×10^{-1}	17	0.11	1100	8.4×10^3

Lubricant thermal properties (SAE 10)

R_o (W/m ² ·K·m)	C_o (N/m ² ·K)	α_o (K/m ²)
1.7×10^{-1}	0.08	0.011

Lubricant viscosity properties (SAE 10)

η		η'
(Pa·s) (oil) (K·m ² /s)	(Pa·s) (oil) (K·m ² /s)	
1.01×10^{-1}	$1.01 \times 10^{-1} \times 10^{-1}$	150

CHAPTER 3 SUMMARY, CONCLUSIONS AND RECOMMENDATIONS

Summary

The study reported in this thesis can be summarized as follows:

Chapter 1 gives a brief review of the surface failure mechanisms such as wear, pitting, roll scoring, and the recent studies on surface failure and gear tooth temperature calculations.

Chapter 2 gives relationship for calculating the nominal temperature rise at the root of contact where the maximum sliding/rolling takes place on the gear tooth surface. This temperature is calculated as transient temperature rise along the contact added to the bulk temperature of gear. The temperature rise, thermal and contact stresses are defined in dimensionless form. Numerical results are also given for several different geometrical conditions such as under/relieve, number of teeth and gear ratio. All these calculations assume smooth surfaces where the base taper is neglected, with a constant coefficient of friction.

Chapter 3 gives the dimensionless relationship for the allowable contact stress modification due to thermal stress. In this chapter, definitions of thermal stress, thermal fatigue and thermal shock are given. The design criteria for the combined mechanical and the thermal stress is given. Two different materials: 1820 low carbon steel and 4040 high carbon steels are considered. Also in this chapter, also the numerical calculations are made under the assumption of constant nominal contact area, constant frictional heat input without consideration of the effect of lubrication film. Further more studies are

input without consideration of the effect of lubrication film. Further stress studies are done for two different cases: one without consideration of the change of viscosity with temperature and the other one with consideration of the effect of this change.

Chapter 4 deals with the investigation of the effect of surface roughness and lubrication. In this chapter, the effect of the lubricating film thickness (given by Dowson and Higginson) and the surface roughness (given by Greenwood-Williamson model) are considered. The study is applied to the gear surface at the first point of contact where the maximum temperature was occurs. Also the evaluation of the coefficient of friction based on the oil film thickness is discussed. A procedure is presented for temperature rise calculation based on the analysis developed by Jindal and Seng. These calculations are undertaken for conditions of boundary lubrication or mixed lubrication depending on the surface roughness and lubricating film thickness. The procedure is applied to rough and fine ground gears with following assumptions, which represent the upper and lower limits of viscosity:

- a) Critical oil viscosity corresponding to the inlet temperature,
- b) Critical oil viscosity corresponding to the maximum bulk surface temperature.

The contact stress modification factors in lubricated rolling/sliding contacts are calculated by using the same approach given in chapter 3 with the consideration of the lubricating film, the gear material and the surface roughness.

Conclusions

The following can be concluded from the reported study:

The surface temperature rise is significantly increased for low number of passes/rev and high gear ratios, as a result of a high sliding to rolling ratio.

The lower number of teeth and higher load consequently decrease the allowable mechanical stress, as shown in equation (3-8).

The allowable mechanical stress is decreased with the decrease in contact distance.

The surface roughness has a significant effect on the temperature rise. Fine ground gears are generally subjected to viscous heating, which reduces the temperature rise at asperities. On the other hand, rough ground surfaces are subjected to frictional heating due to the higher asperity height in relation to the oil film thickness.

The load effect on modeling the allowable contact stress is negligible for conditions of viscous heating.

High carbon steel gears are significantly more sensitive to the thermal stress than low-carbon steel because of the significant changes in their ultimate strength changes with temperature and their high susceptibility to thermal fatigue and thermal shock.

Recommendations

The following are some recommendations for future studies on this subject:

More accurate estimation of the effect of temperature distribution in the contact zone on the viscosity of the lubricating film and the heat generation within the film needs to be considered.

Investigation of the effect of the thermal conditions on the physical and chemical changes which take place in the contact zone.

Investigation of the effect of the electrical system that may be generated on surface as well as surface coating with different thermal properties on the surface temperature.

Planning controlled experiments to verify the general findings of this investigation and to point to any significant parameters that may have not been given adequate consideration in the reported study.

LIST OF REFERENCES

1. Walster, M.N., and Holmstr, C.J.J., "An Experimental Investigation of Microspitting Using a Roller-Gear Machine," *Tribology Trans.*, Vol. 38, 4, pp. 883-893 (1995).
2. Tallian, T.E., "Influence of Asperity Resilience on Surface Deformation and Spalling Life of Resilient Contacts," *Tribology Trans.*, Vol. 38, 1, pp. 28-42, (1995).
3. Tallian, T.E., "Spalling Life Model with Relaxed Distribution Constraints for Rough Rigid-Line Contacts," *ASME Jour. of Tribology*, Vol. 115, 3, pp. 458-468 (1993).
4. Chen, L.Q., "Influence of Contact Temperature on Contact Fringe/Failure Forms: Part I: the Test and Analysis," *ASME Jour. of Tribology*, Vol. 115, 3, pp. 475-479 (1993).
5. Zhou, R.S., Cheng, H.S., and Ma, T., "Microspitting in Rolling and Sliding Contact Under Mixed Lubrication," *ASME Jour. of Tribology*, Vol. 111, 4, pp. 833-837 (1989).
6. Shiao, J.W., and Cheng, H.S., "A Surface Pitting Life Model for Spur-Gears: Part I: Life Prediction," *ASME Jour. of Tribology*, Vol. 113, pp. 705-708 (1991).
7. Shiao, J.W., and Cheng, H.S., "A Surface Pitting Life Model for Spur-Gears: Part II: Failure Probability Prediction," *ASME Jour. of Tribology*, Vol. 113, pp. 713-724 (1991).
8. Shiao, J.W., and Kruger, C.F., "Further Development of a Predictive Pitting model for Gears: Improvements to the Life Prediction Analysis," *STLE Tribology Trans.*, Vol. 37, 2, pp. 137-146.
9. Witten, B., and Orosz, P., "Influence of Lubrication on Pitting and Microspitting Resistance of Gears," *Gear Technology*, Vol. 7, pp. 16-22 (1990).
10. Deng, Y., Jones, B., and Koller, S. B., "Numerical Analysis of Subsurface Crack Initiation Mechanisms From Loss of a Gear Tooth During Engagement," *Wear*, Vol. 181, pp. 141-149 (1995).
11. Lin, J.F., Cheng, M.J., and Deng, P.Y., "Tribological Behaviour of Steel-Rubber Under Rolling-Sliding Contact," *Wear*, Vol. 146, pp. 149-164 (1994).

- 12 Koef, J.A., "Determining the Load-Carrying Progressive Wear-Scuffing) on Gear Transmission," *Soviet Engineering Research*, Vol. 3, 10, pp. 34-37 (1984).
- 13 Mikulinski, S.M., "Ballistics of Involute-Spur Gear Teeth Wear Calculations," *Soviet Jour. of Friction and Wear*, Vol. 8, 1, pp. 38-45 (1985).
- 14 Osadach, Y., Nuchentis, S.P., and Smirnov, S.L., "Development of Methods of Gear (Wheel) Wear Calculations," *Soviet Engineering Research*, Vol. 10, 11, pp. 15-17 (1985).
- 15 Lee, S.C., and Cheng, H.S., "Scuffing Theory Modeling and Experimental Correlations," *ASME Jour. of Tribology*, Vol. 11, pp. 337-338 (1989).
- 16 Lee, S.C., and Cheng, H.S., "Correlation of Scuffing Experiments with EHL Analysis of Rough Surfaces," *ASME Jour. of Tribology*, Vol. 11, pp. 339-336 (1989).
- 17 Lee, S.C., and Chen, H., "Experimental Validation of Critical Temperature-Pressure theory of Scuffing," *Tribology Trans.*, Vol. 18, 1, pp. 734-742 (1995).
- 18 Soudais, Y., "Scuffing of Spur Gear Teeth," *Lubrication Eng.*, Vol. 40, 1, pp. 13-20 (1984).
- 19 Mavroulakis, R.M., "Friction Power as a Criterion of Failure with Sliding Lubricated Contact," *Wear*, Vol. 111, pp. 1-3 (1983).
- 20 Cooper, R.J., and Wu, P.M., "Thermal and Scuffing Behavior of Steels in Sliding Rolling Contact," *ASME Trans.*, Vol. 18, 1, pp. 39-47.
- 21 Bell, J.C., Dwyer, A., and Hadley, J.W., "The Effects of Rolling and Sliding Speeds on the Scuffing of Lubricated Steel Steels," *ASME Trans.*, Vol. 18, 1, pp. 62-70.
- 22 Macpherson, P.B., and Cameron, A., "Fatigue Scoring, a New Form of Lubricant Failure," *ASME Trans.*, Vol. 86, 1, pp. 49-52.
- 23 Townsend, D.P., and Allen, L.B., "Analytical and Experimental Spur-Gear Teeth Temperature as Affected by Operating Variables," *ASME Jour. of Mech. Design*, Vol. 103, pp. 219-226, (1981).
- 24 Ohts, T., Fujita, K., and Fuji, M., "Temperature Rise of a Spur Gear Tooth Due to Repetitive Action of a Sliding Tooth Surface," *Bull. of the JSAE*, Vol. 26, 224, pp. 4481-4488, (1988).
- 25 Ohts, T., Fujita, K., and Fuji, M., "Tooth Temperature Rise of Working Tooth/Pinion in Spur Gears," *JSAE Int. Jour.*, Vol. 20, 262, pp. 571-573, (1987).

26. Rashed, M., and Saeng, A., "Heat Treatment and Treatment Temperature Distribution in Spherical Conspicuous Contacts, Part I: Theoretical Method," *ASME Journal of Tribology*, Vol. 109, pp. 496 (1987).
27. Saeng, A., *Friction and Lubrication in Mechanical Design*, Marcel Dekker, Inc., 1998.
28. Murchison, W. D., "Thermal/Vibrational Mechanical Effects in High Speed Sliding," *Wear*, 79, 4 (1982), pp. 329-343.
29. Manson, S. S., *Thermal Stress and Low-Cycle Fatigue*, McGraw Hill, Inc., New York, 1966.
30. Wang, C. F., "The Effect of Thermal Shock Cycle on Bending Fatigue of High Carbon Steel," M. S. Thesis, Dept. of Mechanical Engineering, University of Wisconsin, Madison, 1960.
31. Collins, J. A., *Fatigue of Materials in Mechanical Design*, John Wiley and Sons, New York, 1981.
32. Cleveland, M., and Lukian, P., *Fatigue of Metallic Materials*, 2nd Ed., Elsevier Science Pub. Co., Inc., New York, 1993.
33. Becker, H., "An Exploratory Study of Stress Concentrations in Thermal Shock Fields," *J. Engg. for Industry*, Trans. ASME, Ser. B, Vol. 84, 1963, pp. 340-348.
34. George, W., *Permanence Gearing: Theory and Practice*, John Wiley and Sons, New York, 1968.
35. Dowson, D., and Higginson, G. R., *Elastohydrodynamic Lubrication*, Pergamon Press, 1966.
36. Hamrock, B. J., and Jacobson, B. O., "Elastohydrodynamic Lubrication of Line Contacts," *ASME Trans.*, Vol. 77, 1954, pp. 175.
37. Wilson, W. R. D., and Shen, S., "Effect of Inlet Shear Heating Due to Sliding on Elastohydrodynamic Film Thickness," *ASME J. of Lubr. Tech.*, Vol. 110, pp. 337 (1988).
38. Albrecht, A. B., "How to Remove Surface Finish in Turning Operations," *Am. Machin.*, Vol. 100, pp. 123-126 (1956).
39. Chandrossen, E. L., and Cook, W. H., "Investigations on the Nature of Surface Finish and Its Variation with Cutting Speed," *Trans. ASME*, Vol. 86, pp. 134-140 (1929).

40. Cohen, R. Y., "Surface Roughness in Torsional Stair Components and its Relevant Mathematical Analysis," *Prod. Eng.*, pp. 293-306 (1984)
41. Jung, D.Y., and Spring, A., "Tool Natural Frequency as the Control Parameter for Surface Roughness," *Mach. Ydr.*, Vol. 1, pp. 147-154 (1992)
42. Hasegawa, M., Spring, A., and Lundberg, R. A., "Surface Roughness Model for Turning," *Technology International*, pp. 285-289 (1996)
43. Bowden, F.P., and Tabor, D., "The Area of Contact Between Stationary and Sliding Surfaces," *Proc. Roy. Soc.*, Vol. 169, No. 933, pp. 384-413 (1939)
44. Archard, J.F., "Contact and Rubbing of Flat Surfaces," *J. Appl. Phys.*, Vol. 34, No. 3, pp. 981-987 (1963)
45. Archard, J.F., "Elastic Deformation and Limits of Friction," *Proc. Roy. Soc. Ser. A*, Vol. 343, No. 1623, pp. 196-207 (1965)
46. Greenwood, J.A., and Williamson, J.B.P., "Contact of Nominally Flat Surfaces," *Proc. R. Soc. London, Ser. A*, 796, pp. 300-313 (1966)
47. McCool, J.L., "Comparison of Models for the Contact of Rough Surfaces," *Wear*, Vol. 107, pp. 37-60 (1988)

BIOGRAPHICAL SECTION

Emrah K. Akar graduated from Fıatlı Technical High School in Konya, Turkey and enrolled in the Department of Mechanical Engineering at Gökten University in Isparta in 1986. After he obtained his engineering degree, he immediately entered the master's program in Energy Technology at the İhsan İsmail Institute of Ege University where he obtained his master's degree in 1993. At the same time, he was awarded a scholarship for postgraduate studies in the U.S. and started a master's program in mechanical engineering at the Illinois Institute of Technology at Chicago in 1994. He obtained master's degree in 1996 and transferred in 1997 to the University of Florida to study for a Ph.D. degree in mechanical engineering. His research is on the thermal effects on surface failures on gears under the direction of Dr. Ali A. Seering. Upon completion of his study, he will start teaching as a faculty in the Department of Mechanical Engineering in İhsan İsmail Institute of Technology in Turkey.

I certify that I have read this study and that in my opinion it conforms to acceptable standards of scholarly presentation and is fully adequate in scope and quality as a dissertation for the degree of Doctor of Philosophy.


Ali A. Ramez, Chairman
Thompson Professor of Mechanical Engineering

I certify that I have read this study and that in my opinion it conforms to acceptable standards of scholarly presentation and is fully adequate in scope and quality as a dissertation for the degree of Doctor of Philosophy.


Carl D. Criss III
Professor of Mechanical Engineering

I certify that I have read this study and that in my opinion it conforms to acceptable standards of scholarly presentation and is fully adequate in scope and quality as a dissertation for the degree of Doctor of Philosophy.


John E. Schwaner
Professor of Mechanical Engineering

I certify that I have read this study and that in my opinion it conforms to acceptable standards of scholarly presentation and is fully adequate in scope and quality as a dissertation for the degree of Doctor of Philosophy.


John C. Zeman
Professor of Mechanical Engineering

I certify that I have read this study and that in my opinion it conforms to acceptable standards of scholarly presentation and is fully adequate in scope and quality as a dissertation for the degree of Doctor of Philosophy.


Edward K. Walsh
Professor of Aerospace Engineering,
Mechanics and Engineering Science

This dissertation was submitted to the Graduate Faculty of the College of Engineering and to the Graduate School and was accepted as partial fulfillment of the requirements for the degree of Doctor of Philosophy

August 2002



Prasad P. Kulkarni
Dean, College of Engineering

Washed M. Phillips
Dean, Graduate School